Bounds on the Coupling Strengths of Communication Channels and their Information Capacities

Zeyu Kuang, David A. B. Miller, and Owen D. Miller

***Abstract*—The concept of optimal communication channels shapes our understanding of wave-based communication. Its analysis typically focuses on specific communication-domain geometries, however, without a general theory of scaling laws or fundamental limits. In this article, we derive shape-independent bounds on the coupling strengths and information capacities of optimal communication channels for any two domains that can be separated by a spherical surface. Previous computational experiments have observed rapid, exponential decay of coupling strengths, but our bounds predict a slower, *sub*-exponential optimal decay, and specific source/receiver distributions that can achieve such performance. Our bounds show that domain sizes and configurations, and not domain shapes, are the keys to maximizing the number of non-trivial communication channels and total information capacities. Applicable to linear time-invariant (LTI) wireless and optical communication systems, our bounds reveal fundamental limits to what is possible through engineering the communication domains of electromagnetic waves.**

***Index Terms*—Communication channels, information capacity, physical bounds, multiple-input–multiple-output (MIMO)**

I. Introduction

OPTIMAL communication channels define the optimal set of sources and measurements for communicating between two volumes [1]–[4]. The total number and relative strengths of the communication channels depend sensitively on the the size and shape of the volumes, which has restricted most studies to specific and often highly symmetric geometries [4]–[26] with only overall sum rules known rigorously for arbitrary shapes [2], [4]. In this article, we identify bounds on the individual coupling strengths between *any* two communication regions, as long as a spherical surface separates them. The bounds depend only on the maximal sizes and minimal separation distances of the two regions, which are typically known a priori (there are fixed regions within which antenna transmitters and receivers can be placed). Our theory leverages a monotonicity property of the singular values of the Green's-function operator to bound the strength of each channel by its analytical counterpart from a concentric bounding volume. A key hypothesis about communication channels has been a seemingly universal exponential decay of the coupling strengths with the channel number, supported in numerous computations [4]–[12], [27]–[30], and which we rigorously prove in two dimensions. Surprisingly, however, we find that such behavior is *not* generic: in three dimensions our bounds decay sub-exponentially, such that their logarithms decrease only with the square root of the channel number and not linearly. The origin of this decay is the additional degeneracies that are possible for concentric domain configurations in three-dimensional space, which underscores the role of dimensionality in channel counting. Our approach leads directly to shape-independent bounds on two fundamental metrics in communication science: the maximal number of non-trivial channels and their information capacities. The bounds show that increasing domain size and optimizing the global configuration, rather than altering the local patterning of the domain shape, are the keys to increasing the number of non-trivial channels and maximizing their information capacities.

Optimal communication channels represent a unifying framework for optical physics [4], [31]–[34] with a wide range of applications in communication sciences [35]–[47]. The Green's-function operator that connects a source volume to a receiver volume, while accounting for all possible background scattering, unambigously dictates the optimal channel profiles and their coupling strengths through its singular vectors and singular values, respectively [1]–[4]. These channels extend previous sampling-theorem-based analyses [48]–[50] from high-symmetry geometries (e.g., regular apertures in the paraxial limit [51], [52], or spheres [53], [54]) to arbitrary ones (see Appendix A in Ref. [4] for a detailed history and discussion of this point). The numerical computation defining these channels—the singular-value decomposition—is sufficiently opaque that analytical insights are still restricted to highly symmetric domains, with little understanding of general properties or scaling laws [4]–[18], [27]–[30] other than overall sum rules [1]–[4].

A classic example that is analytically solvable is the communication between two identical rectangular or circular apertures in the paraxial limit, where the optimal communicating channels are prolate spheroidal waves, exhibiting exponentially decaying coupling strengths [27]–[30]. Similarly rapid decays of channel strengths are observed across different systems, ranging from simple geometries such as rectangular prisms [2], [3], strip objects [5], [13], [14], and concentric circumferences [6], [15], [16], to complex geometries involving conformal conic arcs [7]–[9], [17] and multiple rectilinear or spherical domains [10]–[12], [18]. Many of

This work was supported by Army Research Office under Grant W911NF-19-1-0279 and Air Force Office of Scientific Research under Grant FA9550-171-0002.

Zeyu Kuang and Owen D. Miller are with Department of Applied Physics and Energy Sciences Institute, Yale University, New Haven, Connecticut 06511, USA (email: owen.miller@yale.edu).

David A. B. Miller is with Ginzton Laboratory, Stanford University, 348 Via Pueblo Mall, Stanford, California 94305-4088, USA.

these geometries are reexamined in a recent review paper [4], where numerical observation of apparent exponential decay of coupling strengths past heuristic limits is hypothesized as being possibly universal.

In addition to the channel-strength decay rate, a related open question has been the maximum total number of channels that can be supported between two regions. Identifying bounds on the number of channels has been of interest since the birth of the field [1]–[4], with partial success: channel sum rules imply upper bounds on the number of "well-coupled" channels simply by assumption of a minimum power-measurement threshold and equal division of power among all channels. Yet, as illustrated numerically, for example, in Ref. [4], once we move beyond some simple geometries, such as parallel plane surfaces in a paraxial limit, even well-coupled channels can show substantially different power coupling strengths.

An inspiring precursor to our work is that of Ref. [19]. In Ref. [19], the authors examine the number of communication channels in two dimensions and derive a bound on the number of communication channels between two domains. There is a subtle mathematical issue regarding domain monotonicity (or the lack thereof) of their suggested channel normalization which means that their result is in fact not a fundamental limit (discussed more in Appendix E), but their result can be understood as a heuristic that identifies the correct scaling laws for circular domains in 2D, and roughly maps to the ultimate fundamental limits. The key insight of Ref. [19]—Green's-function singular values have monotonicity properties that imply fundamental limits—forms the foundation of our approach, and enables both the fundamental limits and asymptotic analysis that we identify in two and three dimensions.

The information capacities of optimal communication channels are fundamental to communication sciences and have been investigated for communication domains of various shapes including spherical [15], cubic [55], [56], and non-symmetrical geometries [7], [37]. There are shape-dependent bounds to the information capacities for line-of-sight communications [20]–[24] and spherical communication domains [25], [26]. A more general computational framework is proposed in Refs. [57]–[59] which bounds the information capacity by optimizing over equivalent currents in antenna systems. In this paper, we identify a clean separation between the impedance properties of the antenna networks and the electromagnetic propagation from source to receiver, and identify analytical bounds to the channels over which information can be propagated.

Thus this paper centers around three fundamental questions: how rapidly must optimal communication-channel strengths decay, what is the maximum number of usable communication channels, and what are the consequent bounds on maximum information capacities? To answer these, we first introduce the optimal communication channels in Section II and show their channel strengths satisfy a key "domain monotonic " property, which unlocks a series of upper bounds: maximal channel strengths in 2D (Section III.A) and 3D (Section III.B), the maximal number of non-trivial channels (Section III.C), and their maximal information capacities (Section IV). These results have been previously archived in the leading author's PhD thesis [60].

II. Optimal communication channels

We start by defining communication channels. There are many approaches [1]–[4], [22]–[24], [35]–[37], all of which share a common origin: power can be supplied within a source volume, measured within a receiver volume, and the question is how many *independent*, power-normalized source excitations can be sent to *independent* receivers, and with what strength? The "sources" and "receivers" need not be physically independent antennas; they need only to be orthogonal functions in a suitable basis (such orthogonal signals can be filtered by heterodyne-measurement techniques, for example). Mathematically, the supplied currents $\mathbf{J}_S$ in the source region induce currents $\mathbf{J}_R$ in the receiver region, and we assume a high-resolution discretization such that $\mathbf{J}_S$ and $\mathbf{J}_R$ are vectors with all spatial and polarization degrees of freedom collated. We consider linear electromagnetism, in which case the supplied power P_{supp} and measured power P_{meas} are quadratic forms of $\mathbf{J}_S$ and $\mathbf{J}_R$: $P_{\text{supp}} = \mathbf{J}_S^\dagger \mathbf{R}_S \mathbf{J}_S$ and $P_{\text{meas}} = \mathbf{J}_R^\dagger \mathbf{R}_R \mathbf{J}_R$, where "†" denotes the conjugate transpose, and $\mathbf{R}_S$ and $\mathbf{R}_R$ are generalized resistance matrices (accounting for Ohmic and radiative losses, for example) in the source and receiver regions, respectively. We assume time-invariance in the system properties (not the excitation signals), which implies that no frequency-mixing occurs, and we can consider each frequency independently. (Time-varying backgrounds that vary slowly relative to the signal periods can be treated adiabatically.) The resistance matrices, corresponding to the measurement of real-valued power, are Hermitian and positive semidefinite. They can be factorized into "matrix square roots," e.g. $\mathbf{R}_R = \left(\mathbf{R}_R^{1/2}\right)^\dagger \mathbf{R}_R^{1/2}$, which themselves are positive semidefinite. We exclude non-radiating currents from the source domain since they do not radiate, and hence should not be excited at all. This makes the resistance matrices and their square root positive definite and therefore invertible.

The mapping from supplied currents to measured currents can be broken into three stages. First, by the volume equivalence principle [61], the supplied currents and any complex configuration of antennas, waveguides, substrates, can be replaced by effective currents radiating in the background environment via a linear and possibly nonlocal operator that we denote $\mathbf{T}_S$. These effective currents create the total fields in the receiver location via the background Green's function $\mathbf{G}$. Finally, the total fields map to received currents by another linear and possibly nonlocal operator that we denote $\mathbf{T}_R$. Hence the received currents are related to the supplied currents by the expression $\mathbf{J}_R = \mathbf{T}_R \mathbf{G} \mathbf{T}_S \mathbf{J}_S$, which embodies the linear mapping between currents in two the communication regions.

The optimal communication channels are sets of orthogonal source currents $\mathbf{J}_S$ and their corresponding orthogonal receiver currents $\mathbf{J}_R$, both normalized under certain physical metrics. A natural metric is to normalize the supplied and measured powers: the source current is normalized to unity supplied power $\mathbf{J}_S^\dagger \mathbf{R}_S \mathbf{J}_S = 1$; the receiver current, unity measured power $\mathbf{J}_R^\dagger \mathbf{R}_R \mathbf{J}_R = 1$. To simplify these expressions, one can embed the resistance matrices in two new variables $\mathbf{X}_S = \mathbf{R}_S^{1/2} \mathbf{J}_S$ and $\mathbf{X}_R = \mathbf{R}_R^{1/2} \mathbf{J}_R$, both of which now

enjoy a simple unit norm $\mathbf{X}_S^\dagger \mathbf{X}_S = \mathbf{X}_R^\dagger \mathbf{X}_R = 1$. Under these new variables, the receiver-source connection is given by $\mathbf{X}_R = \mathbf{R}_R^{1/2}\mathbf{T}_R\mathbf{G}\mathbf{T}_S\mathbf{R}_S^{-1/2}\mathbf{X}_S$, and one searches for orthogonal pairs of $\mathbf{X}_S$ and $\mathbf{X}_R$ that defines the optimal communication channels [37]. How to form these pairs is well-known: perform a singular value decomposition (SVD) of the matrix relating $\mathbf{X}_R$ to $\mathbf{X}_S$, which is $\mathbf{R}_R^{1/2}\mathbf{T}_R\mathbf{G}\mathbf{T}_S\mathbf{R}_S^{-1/2}$, with the right singular vectors comprising the orthonormal (basis-transformed) source currents, the left singular vectors comprising the orthonormal receiver currents, and the singular values, $\sigma_n(\mathbf{R}_R^{1/2}\mathbf{T}_R\mathbf{G}\mathbf{T}_S\mathbf{R}_S^{-1/2})$, indicating the strength of the connection—their squares are the powers measured at the receivers for unit-power source excitations.

The generality of this approach, of taking the SVD of $\mathbf{R}_R^{1/2}\mathbf{T}_R\mathbf{G}\mathbf{T}_S\mathbf{R}_S^{-1/2}$, which applies for any set of incoming and outgoing ports, of any material and any dimensionality, also inhibits theoretical understanding. There is essentially no physical system for which the singular values of the five-matrix product can be calculated analytically. Moreover, by encapsulating the full-system coupling, from supplied power to effective source currents, to fields at receivers, and last to the measured power, one can obscure the key bottleneck: the propagation of waves, through free space or any other background environment. There are only so many independent radiation channels that can transport non-trivial amounts of power across sizeable distances (relative to the wavelength). Mathematically, this propagation bottleneck is encapsulated by the following inequality:

$$\sigma_n(\mathbf{R}_R^{1/2}\mathbf{T}_R\mathbf{G}\mathbf{T}_S\mathbf{R}_S^{-1/2}) \leq \sigma_1(\mathbf{R}_R^{1/2}\mathbf{T}_R)\sigma_n(\mathbf{G})\sigma_1(\mathbf{T}_S\mathbf{R}_S^{-1/2}), \tag{1}$$

where we use the fact that $\sigma_n(AB) \leq \sigma_1(A)\sigma_n(B)$ for any matrices A and B. Equation (1) shows that the channel strengths of any physical system must decay at least as fast as the singular values of the Green's function matrix $\mathbf{G}$. The latter, encoding the effect of electromagnetic propagation, is the focus of our paper.

To isolate the effects of propagation, we define our communication channels through the SVD of $\mathbf{G}$ alone, without the extraneous matrices that primarily depend on individual source/receiver properties. Our choice aligns with many previous works [1]–[14], [22]–[24], and it leads to semi-analytical bounds and scaling laws. Our formulation (which relies only on general properties of the Green's function $\mathbf{G}$) can be applied to scenarios with specific $\mathbf{R}_S$, $\mathbf{R}_R$, $\mathbf{T}_S$, and $\mathbf{T}_R$ matrices. One example is given in Appendix, where we compare the channel strengths between two concentric Aluminum antennas (defined by the left hand side of (1)) and those defined by the Green's function alone, and find they decay at the same rate. This shows that the simplified analysis isolating $\mathbf{G}$ generalizes to the full physics of real-material systems.

The central operator that defines our communication channels is the Green's-function operator, $\mathbf{G}$, whose SVD is given by

$$\mathbf{G}(\mathbf{r},\mathbf{r}') = \sum_{q=1}^{\infty} s_q \mathbf{u}_q(\mathbf{r})\mathbf{v}_q^*(\mathbf{r}'), \tag{2}$$

where $\{\mathbf{v}_q(\mathbf{r})\}_{q=1}^{\infty}$ is a set of orthonormal vector-valued basis functions in the source region V_s, $\{\mathbf{u}_q(\mathbf{r})\}_{q=1}^{\infty}$ is a set of orthonormal vector-valued basis functions in the receiver region V_r, and $\{s_q\}_{q=1}^{\infty}$ is the set of (non-negative) singular values. The tuples $\{(\mathbf{v}_q, \mathbf{u}_q, s_q)\}_{q=1}^{\infty}$ are optimal communication channels, with the fields radiated from sources $\mathbf{v}_q(\mathbf{r})$ mapping uniquely to fields $\mathbf{u}_q(\mathbf{r})$ in the receiver region with amplitudes s_q. The absolute square of the amplitude $|s_q|^2$ is referred to as the coupling strength or channel strength of channel q. These channel strengths are only determined by external scatterers in a background environment. It does not depend on the source material (e.g., transmitting antennas) or receiver materials (e.g., detectors), because the former is already replaced by the volume equivalent currents, and the latter we assume does not affect the field propagation. This assumption is observed in many studies [4], [24], [44], and indeed one can expect that any detector effects on the field will primarily be subtractive: dissipating field power or reflecting it away, losing channel strength without gaining any.

The key theorem that enables our shape-independent bounds is that all singular values of a Green's-function operator, as in (2), may not decrease as the source and receiver domains are enlarged [62]. More precisely: if one domain encloses another, each singular value of the former cannot be smaller than the corresponding singular value of the latter. We refer to this property of singular values as "domain monotonicity." It can be proven through a recursive argument. First, the singular values of $\mathbf{G}$ are the square roots of the eigenvalues of $\mathbf{G}^\dagger\mathbf{G}$. Unlike the Green's function $\mathbf{G}$ which typically is not Hermitian (it may not even be square), the operator $\mathbf{G}^\dagger\mathbf{G}$ by construction is always Hermitian, which implies real eigenvalues, and that their eigenvalue/eigenfunction pairs can be found variationally via maximization and orthogonalization. The square of the first singular value of $\mathbf{G}$ is the maximum of the Rayleigh quotient of $\mathbf{G}^\dagger\mathbf{G}$: $|s_1|^2 = \max \frac{\mathbf{p}^\dagger\mathbf{G}^\dagger\mathbf{G}\mathbf{p}}{\mathbf{p}^\dagger\mathbf{p}}$. Clearly this may not decrease as the source domain enlarges, as maximization over a larger space of vectors cannot lead to a smaller optimal value. The second singular value similarly maximizes the Rayleigh quotient, now subject to orthogonality to the first singular vector. Because the first singular vector has changed with the domain, there is not a straightforward comparison to the optimization problem defining the second singular vector of the original domain. Yet the extra freedom given to the first singular vector ultimately only reduces the effect of the orthogonality constraint, such that the second singular value must also increase due to the domain enlargement. (A more precise version of this argument is given in Ref. [63].) The same argument recursively applies to the rest of the singular values, and also for an enlarged receiver domain. (The same argument also extends beyond $\mathbf{G}$ to $\mathbf{R}_R^{1/2}\mathbf{T}_R\mathbf{G}\mathbf{T}_S\mathbf{R}_S^{-1/2}$.) Hence we have the key theoretical ingredients: optimal communication channels are defined by the singular-value decomposition of the Green's-function operator between source and receiver domains, and the singular values satisfy domain monotonicity on both domains.

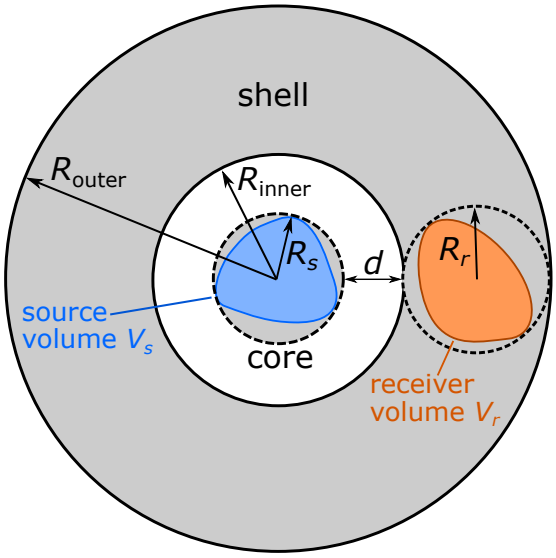

Fig. 1. The coupling strengths of the communication channels between a source volume V_s and a receiver volume V_r are upper bounded by their counterparts from the core–shell bounding volume (shaded in grey). We can also interchange the roles of the source and receiver volumes, and we obtain tighter bounds by using whichever is smaller as the "inner" volume in this figure.

III. Channel-strength bounds

In this section, we derive shape-independent bounds on total channel strengths, relative channel strengths normalized against a sum rule, and their collective asymptotic decay rates in the many-channel limit. The domain-monotonicity principle discussed above immediately leads to bounds: the coupling strengths $|s_q|^2$ for arbitrary source and receiver domains are individually bounded above by the respective coupling strengths of any enclosing domains. Such bounds are tight: they are always attained by filling the enclosing domains with sources and receivers. They generalize a previous bound on the total strength of all channel strengths (a "sum rule") [2] to bounds on individual channel strengths. We select an analytically tractable core–shell set of enclosing domains, depicted as the grey shaded region in Fig. 1, which yield the bounds:

$$|s_q|^2 \leq |s_q^{(\text{core–shell})}|^2, \quad \text{for } q = 1, 2, ... \tag{3}$$

In such core–shell configurations we can choose either the source or the receiver to be enclosed in the core; to find the tightest upper bounds, we take the minimum of both possible configurations. The core is a cylinder for 2D and a sphere for 3D. In the following sub-sections, we derive analytical expressions for the bounds in both dimensions.

A. Channel-strength bounds in 2D

Consider communication in two dimensions between a source domain V_s and a receiver domain V_r as in Fig. 1. The sources are bounded within a cylindrical core of radius R_s and the receivers sit a minimum distance d and maximum distance $d_{\max} = d + 2R_r + 2R_r$ from the sources. The bounding volumes, comprising an inner cylinder and an outer shell, are shaded in grey in Fig. 1. The singular values of the Green's function operator between the concentric cylinder–shell bounding volume can be identified by first performing a separation of variables for the two-dimensional scalar Green's function $G(\mathbf{r}, \mathbf{r}') = \frac{ik^2}{4} H_0^{(1)}(k|\mathbf{r} - \mathbf{r}'|)$ in polar coordinates [64]:

$$G(\mathbf{r}, \mathbf{r}') = \frac{ik^2}{4} \sum_{q=-\infty}^{\infty} H_q^{(1)}(k\rho) e^{-iq\phi} J_q(k\rho') e^{iq\phi'}, \tag{4}$$

where k is the wavenumber, the functions $H_q^{(1)}(k\rho)e^{-iq\phi}$ and $J_q(k\rho)e^{-iq\phi}$ are the outgoing and regular cylindrical waves, with $H_q^{(1)}(x)$ and $J_q(x)$ being the Hankel function of the first kind and the Bessel function, respectively. Their polar coordinates (ρ, ϕ) and (ρ', ϕ') are defined on the bounding shell and bounding cylinder, respectively, relative to the center of the cylinder-shell bounding volume. The cylindrical waves $H_q^{(1)}(k\rho)e^{-iq\phi}$ and $J_q(k\rho)e^{-iq\phi}$ are the (unnormalized) left and right singular vectors of the Green's function operator in the cylinder-shell bounding volume. (The cylindrical symmetry of the bounding volume ensures orthogonality.) There are two possible cylinder–shell bounding volumes: one centers around the source domain and one centers around the receiver domain. To tighten the upper bound, we choose the smaller of the two domains as the "inner" volume in Fig. 1 because it leads to a smaller coupling strength $|s_q^{(\text{cylinder–shell})}|^2$ which is the product of the norms of the unnormalized singular vectors, $H_q^{(1)}(k\rho)e^{-iq\phi}$ and $J_q(k\rho)e^{-iq\phi}$, in their respective bounding volumes:

$$|s_q^{(\text{cylinder–shell})}|^2 = \pi^2 k^2 \int_0^{R_{\min}} |J_q(k\rho)|^2 \rho d\rho \int_{R_{\text{inner}}}^{R_{\text{outer}}} |H_q^{(1)}(k\rho)|^2 \rho d\rho. \tag{5}$$

As the inner bounding cylinder is chosen to encompass the smaller domain, its radius is the smaller of the two radii, i.e., $R_{\min} = \min\{R_s, R_r\}$. Similarly, one can show that the inner and outer radii of the outer bounding shell are $R_{\text{inner}} = d + R_{\min}$ and $R_{\text{outer}} = d + 2R_s + 2R_r - R_{\min}$, respectively. The singular values in (5) are dimensionless quantities because our Green's function, of (4), differs from the conventional definition [4], [65] by a factor of k^2, to be inversely proportional to volume.

The number of non-trivial communication channels is determined by the number of channels whose *relative* channel strengths are above a certain measurement or noise threshold. The relative channel strengths can be normalized either by a total sum rule $S = \sum_{q=-\infty}^{\infty} |s_q|^2$ or by the largest channel strength [4]. Lower bounds on the sum rule can be analytically derived based on the monotonic decay of wave energy in free space, thus leading to bounds on the total number of channels above a certain sum-rule energy fraction. The sum rule S is a double integral of the absolute square of the two-dimensional Green's function over both the source and receiver domains [2], [4]

$$S = \int_{S_s} \int_{S_r} |G(\mathbf{r}, \mathbf{r}')|^2 d\mathbf{r} d\mathbf{r}' \geq k^4 S_s S_r |H_0^{(1)}(k d_{\max})|^2/16, \tag{6}$$

where we further lower bound S by the fact that the magnitude of the Green's function takes its minimal value at the most

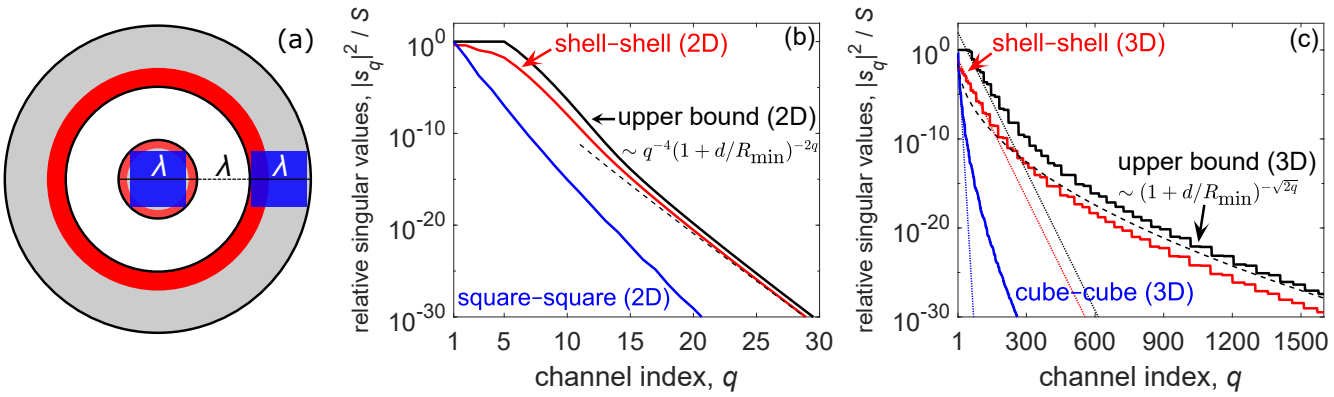

Fig. 2. Shape-independent upper bounds on the relative coupling strengths $|s_q|^2$ normalized against the total sum rule S in two- and three-dimensional spaces. (a) A grey-shaded concentric core–shell bounding volume enclosing a square–square configuration of sources and receivers in the blue shaded region, as well as a shell–shell configuration in the red shaded region. (b) In two-dimensional (2D) space, the upper bound, calculated for the grey-shaded bounding volume in (a), decays exponentially as in the dashed black line. (c) In three-dimensional (3D) space, the additional azimuthal degeneracy leads to an optimal sub-exponential decay that is achieved by the shell–shell configuration. The sub-exponential decay rate (dashed black line) suggests many more communication channels at the large-channel limit than previously hypothesized exponential decays (dotted lines).

separated points between the two domains, which is at a distance $d_{\max} = d+2R_r+2R_s$ for the cylinder–shell bounding volume illustrated in Fig. 1. The variables S_s and S_r in (6) denote the total area of the source and receiver domains. Combining (5) and (6), we derive

$$\frac{|s_q|^2}{S} \leq \frac{16|s_q^{(\text{cylinder–shell})}|^2}{k^4 S_s S_r |H_0^{(1)}(kd_{\max})|^2}, \tag{7}$$

which is a shape-independent bound on the relative channel strength between domains in two-dimensional space. In the many-channel limit, the bound in (7) simplifies:

$$\frac{|s_q|^2}{S} \leq \frac{R_{\min}^4}{q^4 S_s S_r |H_0^{(1)}(kd_{\max})|^2 (1+d/R_{\min})^{2(q-1)}}, \text{as } q \to \infty. \tag{8}$$

The presence of the exponential factor of $2(q-1)$ indicates that channel strengths in two dimensions must decay at least exponentially fast with channel number, in agreement with the previously hypothesized exponential decay of channel strengths. The exponential decay rate depends only on the separation distance d relative to the smaller radius $R_{\min}$ between the two communication domains.

The upper bound in (6) and its optimal exponential decay in (8) applies to any two domains that can be separated by a cylindrical surface. The bound is achieved by concentric communicating domains that fill the bounding volume, while the optimal decay rate can also be achieved with concentric sub-domains. To illustrate the latter point, in Fig. 2(a), we arrange a fixed number of sources and receivers in two different configurations inside a bounding volume. The first configuration (blue shaded region) consists of two squares of sources and receivers with the side lengths of $\lambda/\sqrt{2}$. The second configuration (red shaded region) consists of concentric shell-like communicating domains with the same source and receiver areas. Both configurations are enclosed in a concentric cylinder–shell bounding volume of $2R_s = 2R_r = d = \lambda$. Inside this bounding volume, the maximal relative coupling strength is given by the solid black line in Fig. 2(b), calculated using (7). Compared against it are the coupling strengths from the shell–shell and square–square communicating domains. The former are calculated analytically using (5) with the Bessel integration now bounded by the inner and outer radii of the inner shell. The later are solved numerically by first discretizing the space, then constructing a discretized Green's function matrix using the Hankel-function expression above (4), and last performing numerical singular value decomposition on the Green's function to yield the singular values. We observe that, while the square–square configuration (solid blue line) falls far short of the bound, arranging the same number of sources and receivers to cover a wider solid angle in a shell–shell configuration (solid red line) enables close approach to the upper bound. (The black-line upper bound is clamped to 1; no channel can have strength larger than 1. The looseness of (8) arises from the dramatic mismatch of the source–receiver volumes to the bounding volumes.) Moreover, the shell–shell configuration achieves the optimal exponential decay predicted in (8). This result corroborates previous works [4]–[12], [27]–[30] that predicted exponential decay in wide-ranging scenarios, and hypothesized that exponential decay may be a universal rule. As we show below, however, the three-dimensional behavior is quite different.

B. Channel-strength bounds in 3D

The derivation of shape-independent bounds on channel strengths in three dimensions is similar to the derivation in two dimensions, with the cylinders replaced by spheres. For this 3D case, we now use a vector formulation of the problem, as appropriate for a full electromagnetic solution. So, we move to dyadic Green's functions, and we start by expanding the dyadic Green's function as a summation of outer products, now of spherical vector waves:

$$\mathbf{G}(\mathbf{r},\mathbf{r}') = ik^3 \sum_{n=0}^{\infty} \sum_{m=-n}^{n} \sum_{j=1,2} \mathbf{v}_{\text{out},nmj}(\mathbf{r}) \mathbf{v}_{\text{reg},nmj}^*(\mathbf{r}'), \tag{9}$$

where $\mathbf{v}_{\text{out},nmj}$ and $\mathbf{v}_{\text{reg},nmj}(\mathbf{r}')$ are the outgoing and regular spherical vector waves [66] defined on the bounding shell

and bounding sphere, respectively. The vectors $\mathbf{r}$ and $\mathbf{r}'$ are spherical coordinates defined with respect to the center of the concentric bounding volume. The regular (outgoing) spherical vector waves are formed by combining the angular dependency of vector spherical harmonics with the radial dependency of spherical Bessel (Hankel) functions [66]. Explicit expressions of the spherical vector waves, $\mathbf{v}_{\text{out},nmj}$ and $\mathbf{v}_{\text{reg},nmj}(\mathbf{r})$, and the wave equation we use to define the Green's function are given in Appendix A. The indices n and m index the underlying spherical harmonics, and $j = 1, 2$ denotes the two possible polarizations of a transverse vector field. The orthogonality of the spherical waves in a spherically symmetric domain allows us to identify $\mathbf{v}_{\text{out},nmj}$ and $\mathbf{v}_{\text{reg},nmj}(\mathbf{r})$ as the (unnormalized) left and right singular vectors of the Green's function operator defined on the three-dimensional sphere-shell bounding volumes. The corresponding singular values are the products between the norms of functions $\mathbf{v}_{\text{out},nmj}$ and $\mathbf{v}_{\text{reg},nmj}(\mathbf{r})$ in their respective volumes:

$$|s_{nmj}^{(\text{sphere–shell})}|^2 = k^6 \int_{V_{\text{shell}}} |\mathbf{v}_{\text{out},nmj}(\mathbf{r})|^2 \, d\mathbf{r} \int_{V_{\text{sphere}}} |\mathbf{v}_{\text{reg},nmj}(\mathbf{r})|^2 \, d\mathbf{r}, \tag{10}$$

where V_{shell} and V_{sphere} represent the volumes of the bounding shell and bounding sphere. Explicit expressions of the squared singular values $|s_{nmj}^{(\text{sphere–shell})}|^2$ can be found in Appendix A. According to the domain-monotonicity property in (3), the q-th largest number from the set of all possible squared singular values, $|s_{nmj}^{(\text{sphere–shell})}|^2$, upper-bounds the q-th largest channel strength of any configuration of sources and receivers in the sphere–shell bounding volume.

Again, the number of non-trivial communication channels is determined by normalizing the channel strengths to the total sum rule. The sum rule is now lower bounded by (cf. Appendix C):

$$S = \int_{V_s} \int_{V_r} ||\mathbf{G}(\mathbf{r}, \mathbf{r}')||_F^2 d\mathbf{r} d\mathbf{r}' \geq \frac{k^4 V_s V_r}{8\pi^2 d_{\max}^2} + \mathcal{O}\left((k d_{\max})^{-4}\right). \tag{11}$$

For conciseness, we assume the receivers are far from the sources relative to the wavelength, i.e. $kd_{\max} \gg 1$, so that only the leading term in (11) remains. This can be easily generalized by explicitly including two other higher-order terms, leading to a more complicated expression but the same asymptotic properties.

By combining the upper bound of channel strengths in (3) and the lower bound of the sum rule in (11), we derive a key result for 3D communication domains, a shape-independent upper bound on their relative channel strengths normalized against the total sum rule:

$$\frac{|s_{nmj}|^2}{S} \leq \frac{8\pi^2 d_{\max}^2}{k^4 V_s V_r} |s_{nmj}^{(\text{sphere–shell})}|^2, \tag{12}$$

where the singular value of the sphere–shell bounding volume, $|s_{nmj}^{(\text{sphere–shell})}|^2$, is identified in (10), and whose explicit expression can be found in Appendix A. One immediate prediction of the upper bound in (12) is an optimal sub-exponential decay rate of the channel strengths between two 3D domains, which we now derive. The total number of channels that has n-index less or equal to n is $q = 2(n+1)^2$, because each n-index has

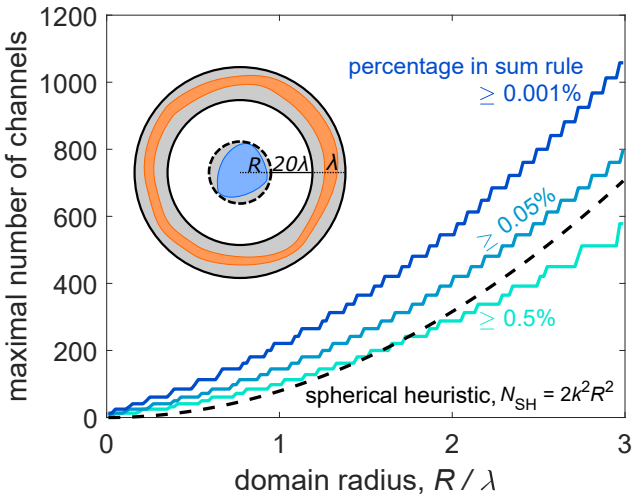

Fig. 3. The maximal number of non-trivial communication channels for a domain of maximal radius R and certain measurement thresholds set by their percentage in the total sum rule. The other communication domain is in a bounding shell shown in the inset. The quadratic dependence of the bound regards to the domain radius R can be conveniently modelled by a spherical heuristic number, $N_{\text{SH}} = 2k^2R^2$.

$2n+1$ m indices (corresponding to unique angular momentum states) and two polarization states. We use this total channel index q as our new index for channel strengths to meaningfully describe their decay rate. When the total number $q \to \infty$, (12) can be simplified to (cf. Appendix D):

$$\frac{|s_q|^2}{S} \leq \frac{2\pi^2 d_{\max}^2}{k^4 V_s V_r (1 + d/R_{\min})^{\sqrt{2q}+1}}, \quad \text{as } q \to \infty, \tag{13}$$

where the parameter $R_{\min} = \min\{R_s, R_r\}$ denotes the radius of the smaller domain. Equation (13) shows that, regardless of the domain shape, channel strengths $|s_q|^2$ in three-dimensional space have to decay at least as fast as $a^{-\sqrt{q}}$, where a is a bounding-domain-dependent numerical constant ($a = (1 + d/R_{\min})^{\sqrt{2}}$), and the key new feature is the square root dependence on q in the exponent. Such a decay is *sub-exponential*, as its logarithm decays only with the square root of the channel number rather than the (much faster) linear reductions characteristic of exponential decay.

Figure 2(c) compares the coupling-strengths bound in 3D, with a clearly sub-exponential decay rate, to the coupling strengths of two configurations of sources and receivers (shell–shell and cube–cube) in a sphere–shell bounding volume. Both configurations possess a volume $\lambda^3/(3\sqrt{3})$ of sources and receivers and follow the same layout as in Fig. 2(a). (Other configurations such as well-separated large domains are studied in Appendix F.) The bounds are calculated via (13); the shell–shell and cube–cube configurations calculated similarly as their 2D counterparts: the former calculated analytically using a modified (10) (the integration of the inner sphere replaced by the inner shell), the latter numerically by performing the singular value decomposition on a discretized Green's function matrix. Similar to the 2D case, we observe that the shell–shell configuration closely follows the bound while the cube–cube configuration falls short. Interestingly,

both the cube-cube and shell-shell configurations and the upper bound first enter a phase of approximately exponential decay (dotted lines in Fig. 2(c), a phenomenon also observed in Ref. [4]) before they exhibit different sub-exponential decays on a larger scale. By "sub-exponential", we mean that the fall off in the channel strengths is not as fast as exponential; high-index channels have somewhat stronger coupling strength than an exponential fall-off would predict. The extent of the benefit of the observed sub-exponential decay depends on the sensitivity of the receivers, as the high-order channels, though abundant, possess small channel strengths relative to the total sum rule. In the many-channel limit, the asymptotic sub-exponential decay predicted in (13) bounds all geometries and also puts forth the concentric shell-shell configurations as the optimal candidate for achieving the slowest sub-exponential decay.

The sub-exponential decay of the channel-strength bound in 3D is in stark contrast with its exponentially decaying counterpart in 2D. This point is accentuated by contrasting Fig. 2(c) with Fig. 2(b), where their asymptotic decay rates, shown as the black dashed lines, are fundamentally different. This difference originates from the possible azimuthal degeneracy of communication channels in 3D. Such degeneracy manifests through the staircase behavior of the upper bound in Fig. 2(c). It allows one to potentially establish many more useful orthogonal channels in 3D: the bound suggests approximately 145 channels for 3D domains above a threshold of 10^{-4} in Fig. 2(c), as compared to only 8 channels in the 2D case above the same threshold. The difference in the decay rate of upper bounds in two- and three-dimensional spaces underscores the role of dimensionality in channel counting.

We have considered in this section source and receiver regions in 3D space, but this does not imply that the sources or receivers need to occupy volumes themselves: they can be surface currents, for example, or even delta-function sources/measurements; all that matters is that they properly normalize to 1. The key role of dimensionality in our results stems from the different number of propagating states that can exist in two versus three dimensions, and has nothing to do with the dimensionalities of the source or receiver distributions.

C. Bounds on the number of non-trivial channels

The number of non-trivial communication channels is often regarded as the number of "spatial degrees of freedom" for communicating between two regions, an idea that generalizes the concept of diffraction limits [4] and dictates fundamental response in many wave systems [32], [67], [68]. A communication channel is considered non-trivial if its coupling strength is above a certain percentage in the total sum rule [4]; the bounds of (7) and (12) on relative coupling strengths therefore directly lead to bounds on the number of communication channels.

Figure 3 shows the maximal number of channels available for any source domain within a three-dimensional sphere of radius R, computed from (12). The receiver domain is a shell twenty wavelengths away, with a thickness of one wavelength, as shown in the inset of Fig. 3. (The source and receiver domains can be transposed.) We also assume both domains occupy at least half of their respective bounding volumes. The bounds are plotted as a function of the maximal domain radius R for a number of measurement thresholds. The bounds are not overly sensitive to the measurement threshold: a five-hundred increase in the sensitivity, as occurs going from the cyan line (0.5%) to the dark blue line (0.001%), does not even double the number of available channels. On the other hand, the bounds increase approximately quadratically with the maximal domain radius R, suggesting enlarging domain size is the key to gaining more useful channels.

The quadratic increase of the bound with respect to the domain radius R can be understood as arising from the increasing surface area of two sufficiently separated communication domains. At first, one might expect the channel number to increase with the *volume* of the domains, but the waves in the volumes are determined by the waves at the surfaces (by the surface equivalence principle [61]), and restrictions on the number of unique wave patterns at the surface will naturally constrain the number of independent volume functions as well. As the domain size increases, we can use the notion of a "spherical heuristic number," denoted N_{SH}, to estimate the number of communication channels:

$$N_{\mathrm{SH}} = 2k^2R^2. \tag{14}$$

This spherical heuristic number, slightly modified from a recent proposed estimate in Ref. [4], dates back to the sampling theorem [54], [69], which estimates the degrees of freedom of an electromagnetic wave to be proportional to the product of its maximal spatial bandwidth and physical extent. It suggests at most two orthogonally polarized channels are possible per λ^2/π area on the surface of a spherical bounding domain. Figure 3 shows quantitative agreement between the spherical heuristic number and the rigorously calculated bound under a 0.05% threshold on the sum rule, explaining the approximately quadratic increase of the number of channels as a function of domain radius.

The bounds in Fig. 3 weakly depend on the sum-rule percentage threshold because of the rapid decay of channel strength at large-order channels. Though not shown in this graph, the bound barely depends on the depth of the receivers and their distance from the source (unless in the extreme near-field limit when the separation distance is much less than a wavelength). All these imply that the group of bounds shown in Fig. 3 represent the intrinsic number of channels one can couple out of any source domain of a given size to well-separated receivers.

IV. Bounds on the Information Capacities of Communication Channels

Information capacity, defined as the maximal rate at which the information can be reliably transmitted between two communicating domains, is a notion that has been central to the development of modern communication systems [37], [48]. In this section, we show how our coupling-strengths bounds identify a maximal information capacity for communication

channels in 3D space, which encapsulates all possible orientations of a 2D antenna plane. As our communication channels concern with only the propagation of electromagnetic waves, the maximal information capacity we derive represent the intrinsic capacity limit of wave propagation.

The intrinsic capacity limit of wave propagation has been previously analyzed in Refs. [22], [24], [56], but all are limited to specific geometries such as rectangular volumes [56] or square surfaces [22], [24]. In contrast, the domain-monotonic property of the channel strengths in Section II allows us to argue a single geometry-independent capacity bound which, computed once for a given bounding volume, applies to all possible geometries within. In addition, unlike the rectangular volumes studied in Ref. [56], we choose a sphere-shell bounding volume which has two favorable attributes: (1) it allows for semi-analytical bounds, (2) the receiver collects all the power emitted from the source so the resulting bound represents the largest information capacity that no further geometric engineering can surpass.

The information capacity C of N optimal communication channels (per unit time and unit bandwidth) is the sum of the capacity of each channel, each of which logarithmically depends on its input power P_q, coupling strength $|s_q|^2$, and noise power P_{noise} [24]:

$$C = \sum_{i=q}^{N} \log_2 \left(1 + \frac{P_q |s_q|^2}{P_{\text{noise}}} \right) \quad \text{bits/s/Hz}, \tag{15}$$

where, following the conventions in both wireless [35], [37] and optical [44], [56] communications, we assume an additive white Gaussian noise background with the same noise power P_{noise} for each channel.

A larger domain size is always favorable to increase the information capacity of the first n optimal communication channels. This is because the capacity C in (15) increases monotonically with coupling strength $|s_q|^2$, which in turn increases monotonically with the domain size. Therefore, the capacity of the sphere–shell bounding volume serves as an upper bound for the capacity of all possible sub-domains within:

$$C \leq \sum_{q=1}^{N} \log_2 \left(1 + \frac{P_q |s_q^{(\text{sphere–shell})}|^2}{P_{\text{noise}}} \right) \quad \text{bits/s/Hz}, \tag{16}$$

where the coupling strength $|s_q^{(\text{sphere–shell})}|^2$ of the sphere–shell bounding volume is given in (10). One can solve for the optimal allocation of powers P_q for a fixed total power input $\sum_{q=1}^{N} P_q = P$, by the "water-filling" algorithm [37], with the semi-analytical form $P_q = \max\{0, \mu - P_{\text{noise}}/|s_q^{(\text{sphere–shell})}|^2\}$, where μ is the numerical constant for which $\sum_{q=1}^{N} P_q = P$. The signal-to-noise ratio (SNR), defined as the ratio between the total power and noise power, i.e. $\text{SNR} = P/P_{\text{noise}}$, is the key external parameter that affects the optimal strategy of the power allocation.

Figure 4 shows the capacity bound for communication between arbitrary domains contained in the sphere–shell bounding volumes in two limits: high SNR (solid black) and low SNR (dashed black). The size dependencies of the capacity

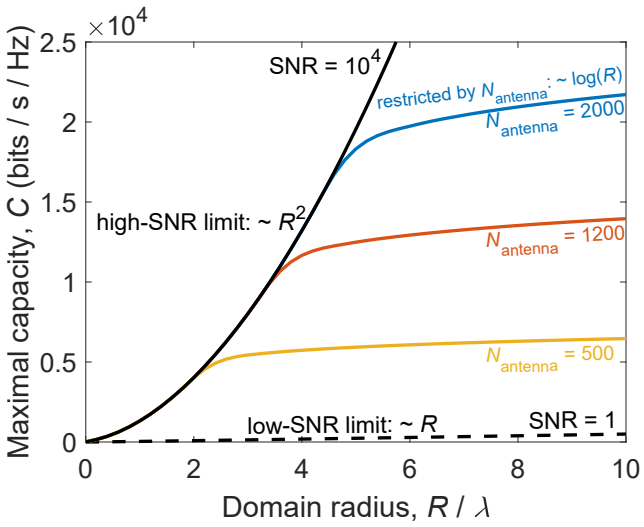

Fig. 4. Maximal information capacity C between any two domains that fit within the radius-R sphere and wavelength-thickness bounding shell of Fig. 3. In the high SNR limit, the bound increases quadratically with domain size R (solid black), whereas in the low SNR limit, the bound increases only linearly (dashed black). When the number of available channels is restricted by the number of antennas, N_{antenna}, the channel-capacity bounds tail off and increase only logarithmically with domain size (blue, orange, yellow).

bounds are quite different in the two limits. When SNR is very small, the logarithms approximately become linear functions of the power, in which case the optimal allocation puts all of the power in the single channel with the highest coupling strength [37]. The maximum coupling strength scales linearly with the radius R: $\max\left\{|s_q^{(\text{sphere–shell})}|^2\right\} = k^2 R_r R$, provided that the radius R of the bounding sphere is much larger than a wavelength and the bounding shell far from the bounding sphere (cf. Appendix B). Then we have

$$C \leq \text{SNR} \cdot \log_2(e) k^2 R_r R, \quad \text{for} \ \ \text{SNR} \to 0. \tag{17}$$

By contrast, in the high-SNR limit, the optimal allocation of power equally divides among all channels with nonzero channel strengths [37]. The information capacity in this case scales with the number of such channels, which, as we established in the Sec. IV, depends quadratically with the domain radius R (modeled by the spherical heuristic number $N_{\text{SH}} = 2k^2R^2$). Hence, the capacity bound increases quadratically with R in the high-SNR limit:

$$C \leq 2 \log_2(\text{SNR}) k^2 R^2, \quad \text{for} \ \ \text{SNR} \gg 0. \tag{18}$$

In many scenarios, the number of communication channels may be restricted well below our electromagnetic limit; one common example may be a MIMO system with antennas spaced more than half a wavelength apart. When the number of communication channels is restricted by the number of antennas, N_{antenna}, the growth in the large-domain limit cannot remain quadratic or even linear; instead, the capacity bound will grow logarithmically at best. This is because for a fixed number of channels, the capacity of each channel increases

logarithmically with channel strength, which in turn increases at most linearly with R:

$$C \leq N_{\text{antenna}} \log_2 \left(\text{SNR} \cdot \frac{k^2 R_r R}{N_{\text{antenna}}} \right), \quad \text{for} \ \ \text{SNR} \gg 0. \tag{19}$$

The logarithmic dependence is confirmed by the computations of the blue, orange, and yellow lines in Fig. 4, with each having the same SNR as the solid black line, but decreasing N_{antenna}. The quadratic increase at the outset of each curve saturates almost exactly at the domain size where the number of electromagnetic channels ($N_{\text{SH}} = 2k^2R^2$) equals N_{antenna}. Thus, despite the abundant number of electromagnetic channels in a large domain, antenna restrictions can impose significant constraints on the total information capacity.

V. Extensions

The key finding in this paper is a shape-independent bound on coupling strengths that we derive based on the domain-monotonicity property of the Green's function operator. This upper bound leads to two important discoveries. First, the sub-exponential decay in (13) identifies the slowest possible decay rate between any two domains in free space, and implies that three-dimensional domains have dramatically more channels available than their two-dimensional counterparts. Second, the ensuing bounds and scaling laws on the maximal number of usable communication channels and their maximal N-channel information capacity represent the ultimate limit that no domains can surpass. In this section, we briefly touch on other possible extensions of these results.

The bounding volume for the source and receiver domains can be any shape and size. We choose the concentric bounding volume in this article because of its analyticity and generality: its singular values are analytically tractable and the resulting bound is general enough to apply to any two domains that can be separated by a spherical surface. In practice, if the sources and receivers are constricted to a domain smaller than the concentric bounding volume, one can sacrifice the analyticity by numerically computing the singular values of the largest possible domain for a tighter bound. Another analytical though less general bounding volume arises when the sources and receivers are known to be in the paraxial limit. Then, one can form the bounding volume as two rectangular cuboids whose singular values are known analytically in the paraxial limit [2]. While we mainly focus on the concentric sphere–shell bounding volume in this work, future studies of alternative bounding volumes may reveal the dependence of the bound on the solid angles between the sources and receivers that otherwise cannot be captured by a concentric bounding volume.

The n-channel capacity bound proposed in this article may have ramifications on the optimal performance of antenna selection in massive multiple-input and multiple-output (MIMO) systems [70]–[73]. The technique of antenna selection mitigates the cost and complexity of MIMO systems by judiciously selecting only a fixed-size subset of antennas while maintaining a large total information capacity. How large the total information capacity can be among all the possible subsets is a question that falls under the umbrella of our N-channel capacity bound, which suggests the possibility to bound the capacity of any N-antenna subset by the capacity of the first N optimal channels of the total antenna arrays.

Our model, assuming a deterministic scattering system whose Green's function operator is known and fixed, can be extended to cases where the exact location of the scatterer is unknown but governed by certain probability distributions, such as in geometry-based stochastic models [74], [75] or optical scattering in random media [38], [40]. In the simplest case, we can assume there are a number of possible scatterer configurations, each occurring with a possibility p_i and characterized by a unique Green's function operator $\mathbf{G}_i$. The operator $\sum_i p_i \mathbf{G}_i^\dagger \mathbf{G}_i$ measures average power transmission in this environment. Its first n eigenvectors define the first n optimal communication channels of such a stochastic system. The operator $\sum_i p_i \mathbf{G}_i^\dagger \mathbf{G}_i$ is subject to the same monotonicity theorems described in Section II, and generalizes our approach from deterministic scattering settings to stochastic ones.

Temporally modulating external scatterers presents unique theoretical challenges but also tantalizing rewards [76]–[78]. This paper assumes a linear time-invariant system so that each frequency communicates independently. Once the external scatterer is modulated in time, one frequency excited in the input can induce another frequency in the output. The induced second frequency may strongly interfere with the original second frequency that comes directly from the excitation, leading to potentially richer channel paths and stronger channel strengths. The extent of this interference may be analyzed by building a Green's function matrix $\mathbf{G}$ that includes not only spatial dimensions but also a new spectral dimension [76]. The "off-diagonal" components in the spectral dimension of $\mathbf{G}$ represent the inter-frequency coupling induced by temporal modulation. The singular value decomposition of such modified Green's function $\mathbf{G}$ may reveal the optimal spatial and spectral distributions of the input signal that maximize the information throughput in a time-modulated system.

Geometrically patterning external scatterers may also enhance the scattering amplitude of electromagnetic fields and its total information throughput. There are many shape-independent bounds proposed in this regard to bound the maximal power response of such external scatterers [67], [68], [79]–[93], though there is still a need to understand their maximal information throughput. For example, to what degree could an external scatterer alter the sub-exponential decay rate predicted in this paper? What is the maximal number of non-trivial channels an external scatterer can help to establish and what are the maximal information capacities of those channels? Though a few bounds have been identified in certain physical scenarios [32], [33], [94], [95], those are still open questions that await for general answers. Among various design techniques in search of better scatterer structures or antenna arrays, shape-independent bounds continue to offer a new lens to analyze the fundamental limits of information and power transfer in both fundamental physics and communication science.

During the publication process of this manuscript, two

recent works from Gustafsson [96], [97] develop channel-counting heuristics that are rigorously correct in the geometric-optics (short-wavelength) limit.

APPENDIX A
SINGULAR VALUES OF THE GREEN'S FUNCTION OPERATOR IN THE SPHERE–SHELL BOUNDING VOLUME

The dyadic Green's function $\mathbf{G}(\mathbf{r},\mathbf{r}')$ is defined as the solution of the following wave equation under a point source excitation: $\frac{1}{k^2}\boldsymbol{\nabla}\times\boldsymbol{\nabla}\times\mathbf{G}(\mathbf{r},\mathbf{r}')-\mathbf{G}(\mathbf{r},\mathbf{r}')=\mathbf{I}\delta(\mathbf{r}-\mathbf{r}')$, where $\mathbf{I}$ is the unit dyad and k is the magnitude of the free-space wavevector. Its solution $\mathbf{G}(\mathbf{r},\mathbf{r}')=(k^2\mathbf{I}+\nabla\nabla)\frac{e^{ik|\mathbf{r}-\mathbf{r}'|}}{4\pi|\mathbf{r}-\mathbf{r}'|}$ can be expanded by the outgoing and regular spherical vector waves [66]:

$$\mathbf{G}(\mathbf{r},\mathbf{r}')=ik^3\sum_{n=0}^{\infty}\sum_{m=-n}^{n}\sum_{j=1,2}\mathbf{v}_{\mathrm{out},nmj}(\mathbf{r})\mathbf{v}^{*}_{\mathrm{reg},nmj}(\mathbf{r}'), \tag{20}$$

where $\mathbf{v}_{\mathrm{out},nmj}(\mathbf{r})$ and $\mathbf{v}_{\mathrm{reg},nmj}(\mathbf{r}')$ denote the two types of spherical vector waves. The index n and m are the two indices of the underlying spherical harmonics, and $j=1,2$ denotes the two possible polarizations of the transverse vector field.

The spherical vector waves can be separated into a radial dependency of a spherical Hankel/Bessel function and an angular dependency of vector spherical harmonics:

$$\mathbf{v}_{\mathrm{out},nm1}(\mathbf{r})=\gamma_n h_n^{(1)}(kr)\mathbf{V}^{(3)}_{nm}(\theta,\phi) \tag{21}$$

$$\mathbf{v}_{\mathrm{out},nm2}(\mathbf{r})=\gamma_n\left\{n(n+1)\frac{h_n^{(1)}(kr)}{kr}\mathbf{V}^{(1)}_{nm}(\theta,\phi)+\frac{\left[krh_n^{(1)}(kr)\right]'}{kr}\mathbf{V}^{(2)}_{nm}(\theta,\phi)\right\} \tag{22}$$

$$\mathbf{v}_{\mathrm{reg},nm1}(\mathbf{r})=\gamma_n j_n(kr)\mathbf{V}^{(3)}_{nm}(\theta,\phi) \tag{23}$$

$$\mathbf{v}_{\mathrm{reg},nm2}(\mathbf{r})=\gamma_n\left\{n(n+1)\frac{j_n(kr)}{kr}\mathbf{V}^{(1)}_{nm}(\theta,\phi)+\frac{[krj_n(kr)]'}{kr}\mathbf{V}^{(2)}_{nm}(\theta,\phi)\right\}, \tag{24}$$

where (r,θ,ϕ) are the spherical coordinates centered at the center of our sphere–shell bounding volume, and the prefactor $\gamma_n=1/\sqrt{n(n+1)}$. The three vector spherical harmonics are an extension of the scalar spherical harmonics: $\mathbf{V}^{(1)}(\theta,\phi)=\hat{r}Y_n^m(\theta,\phi)$, $\mathbf{V}^{(2)}(\theta,\phi)=r\nabla[Y_n^m(\theta,\phi)]$, and $\mathbf{V}^{(3)}(\theta,\phi)=\nabla\times[\hat{r}Y_n^m(\theta,\phi)]$, where $Y_n^m(\theta,\phi)=\sqrt{\frac{(2n+1)(n-m)!}{4\pi(n+m)!}}P_n^m(\cos\theta)e^{im\phi}$ are the scalar spherical harmonics defined by associated Legendre polynomials $P_n^m(x)$. The radial dependency of the outgoing spherical vector harmonics are the spherical Hankel function of the first kind, $h_n^{(1)}(kr)$, with the domain of r restricted to the region of the bounding shell. The radial dependency of the regular spherical vector harmonics are the spherical Bessel function $j_n(kr)$, with the domain of r restricted to the region of the bounding sphere.

The three vector spherical harmonics, $\mathbf{V}^{(1)}_{nm}(\theta,\phi)$, $\mathbf{V}^{(2)}_{nm}(\theta,\phi)$, and $\mathbf{V}^{(3)}_{nm}(\theta,\phi)$, satisfy the following orthogonal property: $\int_0^{\pi}d\theta\sin\theta\int_0^{2\pi}d\phi\mathbf{V}^{(\alpha)}_{nm}(\theta,\phi)\cdot\mathbf{V}^{(\beta)*}_{n'm'}(\theta,\phi)=z_{\alpha n}\delta_{\alpha\beta}\delta_{mm'}\delta_{nn'}$, where the prefactor $z_{1n}=1$ and $z_{2n}=z_{3n}=n(n+1)$. This condition ensures outgoing/regular spherical vector waves are orthogonal in the bounding shell/sphere. Therefore, we identify these two as the left and right singular vectors of the Green's function operator in the sphere–shell bounding volume.

Equation (20) can be interpreted as the singular value decomposition of the Green's function. The singular values are the products between the norms of the unnormalized singular vectors $\mathbf{v}_{nmj}(\mathbf{r})$ and $\mathrm{Rg}\mathbf{v}_{nmj}(\mathbf{r})$ in their respective domains:

$$|s^{(\text{sphere–shell})}_{nmj}|^2=k^6\int_{V_{\text{sphere}}}|\mathbf{v}_{\mathrm{reg},nmj}(\mathbf{r})|^2\,d\mathbf{r}\int_{V_{\text{shell}}}|\mathbf{v}_{\mathrm{out},nmj}(\mathbf{r})|^2\,d\mathbf{r}. \tag{25}$$

Plugging in $\mathbf{v}_{\mathrm{reg},nmj}(\mathbf{r})$ and $\mathbf{v}_{\mathrm{out},nmj}(\mathbf{r})$ from (21 – 24), we can show:

$$|s^{(\text{sphere–shell})}_{nm1}|^2=\frac{\pi^2}{16}x^2\left[J^2_{n+\frac{1}{2}}(x)-J_{n+\frac{3}{2}}(x)J_{n-\frac{1}{2}}(x)\right]\Big|_{x=0}^{x=kR_{\text{sphere}}}\times y^2\,\mathrm{Re}\left[|H^{(1)}_{n+\frac{1}{2}}(x)|^2-H^{(1)}_{n+\frac{3}{2}}(y)H^{(2)}_{n-\frac{1}{2}}(y)\right]\Big|_{y=kR_{\text{inner}}}^{y=kR_{\text{outer}}} \tag{26}$$

$$\begin{aligned}|s^{(\text{sphere–shell})}_{nm2}|^2=\frac{\pi^2}{16}x^2\Bigg\{&\frac{n+1}{2n+1}\left[J^2_{n-\frac{1}{2}}(x)-J_{n+\frac{1}{2}}(x)J_{n-\frac{3}{2}}(x)\right]\\&+\frac{n}{2n+1}\left[J^2_{n+\frac{3}{2}}(x)-J_{n+\frac{5}{2}}(x)J_{n+\frac{1}{2}}(x)\right]\Bigg\}\Big|_{x=0}^{x=kR_{\text{sphere}}}\\&\times y^2\,\mathrm{Re}\Bigg\{\frac{n+1}{2n+1}\left[|H^{(1)}_{n-\frac{1}{2}}(y)|^2-H^{(1)}_{n+\frac{1}{2}}(y)H^{(2)}_{n-\frac{3}{2}}(y)\right]\\&+\frac{n}{2n+1}\left[|H^{(1)}_{n+\frac{3}{2}}(y)|^2-H^{(1)}_{n+\frac{5}{2}}(y)H^{(2)}_{n+\frac{1}{2}}(y)\right]\Bigg\}\Big|_{y=kR_{\text{inner}}}^{y=kR_{\text{outer}}},\end{aligned} \tag{27}$$

where the functions $J_n(x)$ and $H_n^{(1)}(x)$ denote the Bessel function and the Hankel function of the first kind. Equations (26, 27) are the explicit expressions of $|s^{(\text{sphere–shell})}_{nmj}|^2$ we use in the paper to calculate the upper bounds of the coupling strengths between any two regions in the bounding volume.

APPENDIX B
MAXIMAL CHANNEL STRENGTH IN THE LIMITS OF LARGE BOUNDING SPHERE AND WELL-SEPARATED BOUNDING SHELLS

We observe that the maximal channel strength in the sphere–shell bounding domain is asymptotically attained by the first angular channel of the second polarization state in the limit of large bounding sphere:

$$\max|s^{(\text{sphere–shell})}_{nmj}|^2=|s^{(\text{sphere–shell})}_{002}|^2,\quad\text{for } R_{\text{sphere}}\gg\lambda, \tag{28}$$

This is evidenced by Fig. 5, which shows that the relative difference between $\max|s^{(\text{sphere–shell})}_{nmj}|^2$ and $|s^{(\text{sphere–shell})}_{002}|^2$ is smaller than 5% for a bounding sphere with radius R_{sphere} larger than three times the wavelength λ and the relative difference asymptotically tends to zero as the radius becomes much larger than the wavelength. The separation distance d between the two bounding domains and the maximal thickness

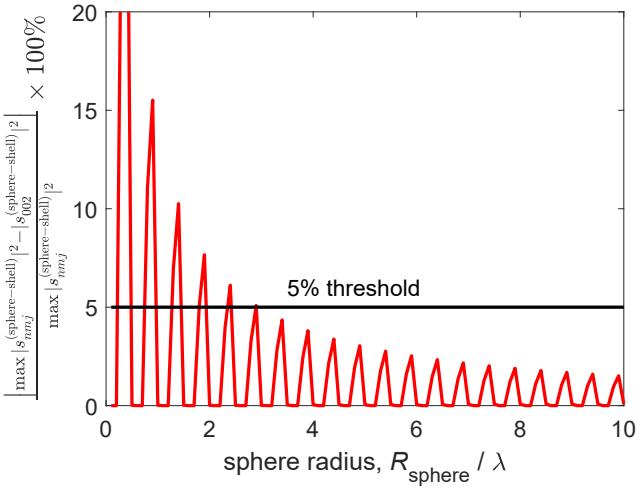

Fig. 5. Numerical evidence showing that the maximum channel strength, $\max|s_{nmj}^{(\text{sphere–shell})}|^2$, is asymptotically attained by the first angular channel of the second polarization state, $|s_{002}^{(\text{sphere–shell})}|^2$, in the limit of large sphere radius R_s relative to the free-space wavelength λ.

$2R_r$ of the spherical shell is assumed to be 10λ and λ, respectively, though our result does not appear to be sensitive to these two parameters.

The channel strength $|s_{002}^{(\text{sphere–shell})}|^2$ has a simple analytical form in the limits of large bounding sphere and well-separated bounding shell. Specifically, in the limit of a well-separated bounding shell, $|s_{002}^{(\text{sphere–shell})}|^2$ simplifies to

$$|s_{002}^{(\text{sphere–shell})}|^2 = 2kR_r \int_0^{kR_{\text{sphere}}} x^2 |j_{-1}(x)|^2 dx, \quad \text{for } d \gg \lambda, . \tag{29}$$

Furthermore, the integral in (29) can be analytically evaluated considering that $j_{-1}(x) = \cos(x)/x$. Its result, under the limit of large bounding sphere, reduces to

$$|s_{002}^{(\text{sphere–shell})}|^2 = k^2 R_r R_{\text{sphere}}, \text{ for } R_{\text{sphere}} \gg \lambda \text{ and } d \gg \lambda. \tag{30}$$

Combining (28) and (30), we derive an analytical expression of the maximal channel strength in the limits of large bounding sphere and well-separated spherical shell:

$$\max|s_{nmj}^{(\text{sphere–shell})}|^2 = k^2 R_r R_{\text{sphere}} \tag{31}$$

for $R_{\text{sphere}} \gg \lambda$ and $d \gg \lambda$, which, we observe, scales linearly with the maximal radii of both the source and receiver domains.

APPENDIX C
A LOWER BOUND ON THE SUM RULE

The sum rule $S = \sum_{nmj} |s_{nmj}|^2$ is conserved under a unitary transformation from the communication channel basis to the delta-function basis in real space. Conveniently, we express S as a double integral of the Frobenius norm of the dyadic Green's function over both the source and receiver volumes:

$$S = \int_{V_s} \int_{V_r} ||\mathbf{G}(\mathbf{r}, \mathbf{r}')||_F^2 d\mathbf{r} d\mathbf{r}'. \tag{32}$$

The Frobenius norm of the dyadic Green's function reads [85]

$$||\mathbf{G}(\mathbf{r}, \mathbf{r}')||_F^2 = \frac{k^6}{8\pi^2} \left[\frac{1}{(k|\mathbf{r} - \mathbf{r}'|)^2} + \frac{1}{(k|\mathbf{r} - \mathbf{r}'|)^4} + \frac{3}{(k|\mathbf{r} - \mathbf{r}'|)^6} \right] \tag{33}$$

which monotonically decays with respect to the separation distance, $|\mathbf{r} - \mathbf{r}'|$, between two points. This monotonic decay allows us to lower bound the sum rule by relaxing the separation distance to the largest possible separation distance, $\max|\mathbf{r} - \mathbf{r}'| = d + 2R_s + 2R_r$, between the source and receiver volumes:

$$S \geq \frac{k^4 V_s V_r}{8\pi^2 (d + 2R_s + 2R_r)^2} + \mathcal{O}\left([k(d + 2R_s + 2R_r)]^{-4} \right). \tag{34}$$

The variables R_s and R_r denote the maximal radii of the source and receiver domains. For conciseness, we assume the receivers are far away from the sources, i.e. $k(d + 2R_s + 2R_r) \gg 1$, so that only the leading term in (34) remains. This, of course, can be easily generalized by explicitly including two other higher-order terms with a slightly more complicated expression.

APPENDIX D
AN UPPER BOUND ON THE RELATIVE COUPLING STRENGTHS IN THE LARGE-CHANNEL LIMIT

The singular values $|s_{nmj}^{(\text{sphere–shell})}|^2$ have simple analytical expressions in the large-channel limit when the index $n \to \infty$. They can be derived by substituting the large-n asymptotes of the Bessel and Hankel functions into (26, 27), yielding:

$$|s_{nm1}^{(\text{sphere–shell})}|^2 = \left(\frac{kR_{\text{sphere}}}{2n} \right)^4 \left(\frac{R_{\text{sphere}}}{R_{\text{inner}}} \right)^{2n-1} \quad \text{as } n \to \infty, \tag{35}$$

$$|s_{nm2}^{(\text{sphere–shell})}|^2 = \frac{1}{4} \left(\frac{R_{\text{sphere}}}{R_{\text{inner}}} \right)^{2n+1} \quad \text{as } n \to \infty. \tag{36}$$

While both polarizations decay exponentially as a function of n, the first polarization channel is always smaller than the second one in the large n limit due to the additional decay of the factor of $1/n^4$. The value of the second polarization thus serves as an upper bound for both:

$$|s_{nmj}^{(\text{sphere–shell})}|^2 \leq \frac{1}{4} \left(\frac{R_{\text{sphere}}}{R_{\text{inner}}} \right)^{2n+1} \quad \text{as } n \to \infty. \tag{37}$$

This is an upper bound for the coupling strengths of both polarizations in a sphere–shell bounding volume in the large-channel limit. The bound only depends on the ratio between the radius of the bounding sphere, R_{sphere}, and the inner radius of the bounding shell, R_{inner} — the smaller the ratio, the faster the decay.

For any two domains that can be separated by a spherical surface, there are two possible sphere–shell bounding volumes: one that centers around the source region and one that centers around the receiver region. To obtain a tighter upper bound, we choose the one that centers around the smaller domain because it has the smaller ratio between R_{sphere} and R_{inner}. Considering

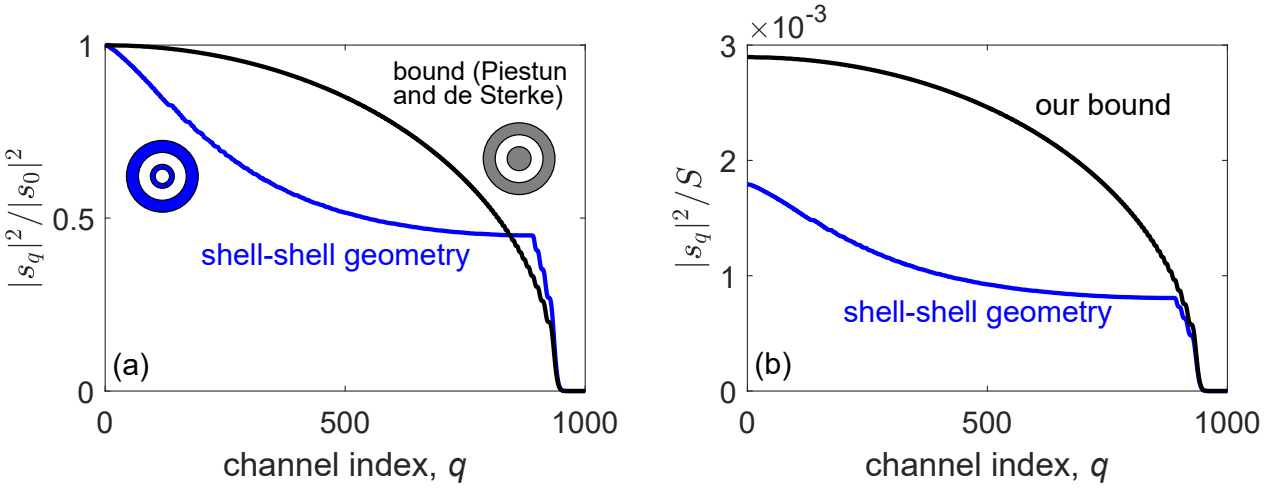

Fig. 6. A shell–shell structure (blue-colored inset) that violates the propsed bound by Piestun and de Sterke in Ref. [19]. (b) The relative coupling strength $|s_l|^2/|s_0|^2$ of the shell–shell geometry, normalized by the 0-th order coupling strength, violates the proposed bound by Piestun and de Sterke [19] which are their counterparts in the cylinder–shell bounding volume (grey-colored inset). (c) The relative coupling strength $|s_l|^2/S$ from the same shell–shell structure, normalized by the sum rule, is correctly bounded in our approach.

this and the fact that the number of channels with n-index less or equal to n is $q = 2(n+1)^2$, (37) can be written as

$$|s_q^{(\text{sphere–shell})}|^2 \leq \frac{1}{4}\left(1+\frac{R_{\min}}{d}\right)^{-\sqrt{2q}-1} \quad \text{as } q\to\infty, \quad (38)$$

where $R_{\min} = \{R_s, R_r\}$ is the smaller of the radius of the source domain R_s and the radius of the receiver domain R_r, and d is the distance between the two domains. This equation shows the coupling strengths between two regions always decay *sub*-exponentially with the total channel index, q, in the large-channel limit.

Lastly, we invoke the domain-monotonicity theorem discussed in Section II of the paper which implies that the coupling strengths $|s_q|^2$ between any two domains have to be smaller than their counterparts in a sphere–shell bounding volume:

$$|s_q|^2 \leq |s_q^{(\text{sphere–shell})}|^2, \quad \text{for } q = 1, 2, \ldots \quad (39)$$

Combining this with the upper bound of $|s_q^{(\text{sphere–shell})}|^2$ in (38) and the lower bound of the sum rule S in (34), we derive an upper bound on the relative channel strengths in the large-channel limit:

$$\frac{|s_q|^2}{S} \leq \frac{2\pi^2(d+2R_s+2R_r)^2}{k^4 V_s V_r (1+d/R_{\min})^{\sqrt{2q}+1}}, \quad \text{as } q\to\infty. \quad (40)$$

This suggests that the relative coupling strength between any two domains decay at least sub-exponentially in the large-channel limit. Equation (40) is a key result presented in our paper and we hereby provide a derivation in this section.

APPENDIX E
COMPARISON WITH THE RESULTS OF PIESTUN AND DE STERKE

Piestun and De Sterke [19] have analyzed concentric cylindrical objects to obtain a first approximate analysis of the numbers of well-coupled communications channels in two dimensions, in the limit of well-separated receivers and large source domains. The reason it is an approximation, not a exact bound, is because of two assumptions they made. First, they assume, for all geometries, the channel strengths $|s_q|^2$ are constant up to a certain channel index, after which the channel strengths fall off rapidly. Second, they assume, for all geometries, their relative channel strengths $|s_q|^2/|s_0|^2$ are upper bounded by their counterparts in the cylinder–shell bounding volume, $|s_q^{(\text{cylinder–shell})}|^2/|s_0^{(\text{cylinder–shell})}|^2$. (This assumption, though not explicitly stated in Ref. [19], arises when its (6) is used for upper bounds.) Under these two assumptions, they derive an upper bound on the number of well-coupled channels, N, in a cylinder–shell bounding volume:

$$N \approx \sum_{q=-\infty}^{\infty} \frac{|s_q|^2}{|s_0|^2} \leq \sum_{q=-\infty}^{\infty} \frac{|s_q^{(\text{cylinder–shell})}|^2}{|s_0^{(\text{cylinder–shell})}|^2}. \quad (41)$$

This expression is meaningful for (circular) cylinders, but is not a "fundamental limit" for any shape. In order for the inequality in (41) to be valid, one would need the denominator on the right, the first singular value of the cylinder, to be less than or equal to the denominator on the left, the first singular value of any arbitrary domain. Yet this inequality is not valid in general, not even in their assumed well-separated-receiver large-source limit. One geometry that violates the singular-value inequality is a "shell–shell" geometry that consists of two concentric cylindrical shells as shown in the blue-colored inset of Fig. 6(a). Its normalized channel strengths, $|s_q|^2/|s_0|^2$, are plotted as the blue line for the first 1000 channels. We assume the inner cylindrical shell has inner and outer radii of 100λ and 150λ, and the outer cylindrical shell has inner and outer radii of 1000λ and 1100λ. A part of the blue line surpasses the supposed upper bound (black line) given by the normalized channel strengths, $|s_q^{(\text{cylinder–shell})}|^2/|s_0^{(\text{cylinder–shell})}|^2$, of the cylinder–shell bounding volume.

On the other hand, the approach presented in our paper correctly bounds the response from the same shell–shell ge-

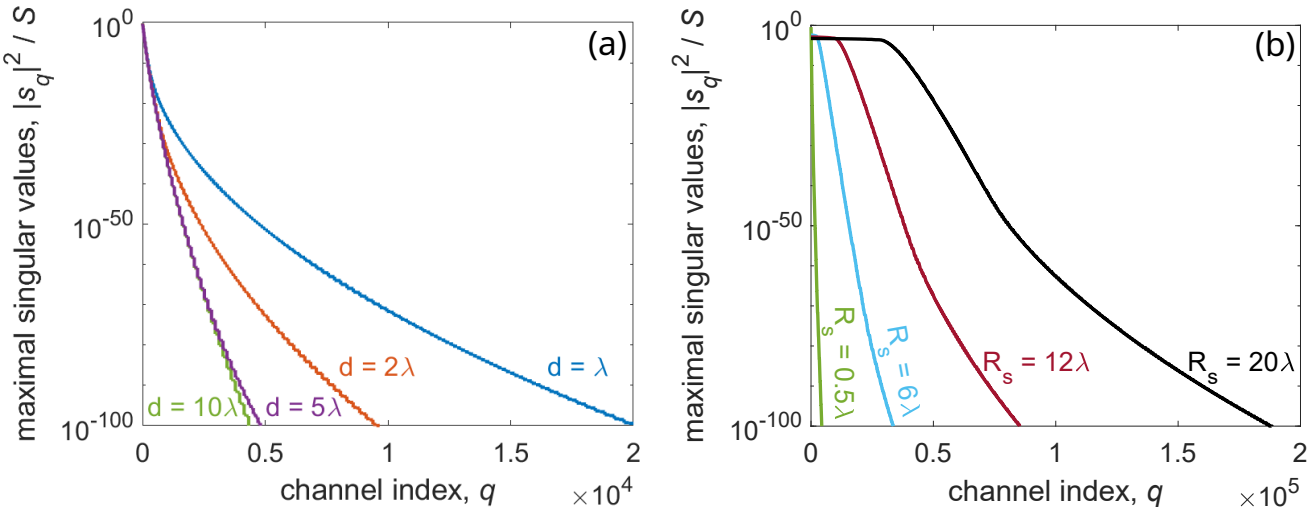

Fig. 7. Maximal channel strengths between two domains for various (a) separation distances d and (b) source domain radii R_s. In both cases, we assume the receiver domain has $R_r = 0.5\lambda$ and the filling ratio is at least fifty percent. We find the sub-exponential decay is most prominent when channels are abundant as in the case of communicating at moderate separations (the blue line in (a)) or between large domains (the black line in (b)).

ometry at each channel, as shown in Fig. 6(b). Our bound is a rigorous upper bound to all geometries because we do not make any prior assumptions on the domain configurations or their singular values. We do not assume well-separated receivers, nor large source domains. We do not assume a step-like distribution of the channel strengths (as in Ref. [19]). We also employ a sum-rule normalization where the relative channel strengths can always be bounded above.

APPENDIX F
SUB-EXPONENTIAL DECAYS FOR VARIOUS DOMAIN SIZES AND SEPARATION DISTANCES

In the main text, we show that maximal coupling strengths decay sub-exponentially in three dimensions. In this section, we investigate how such sub-exponential decay changes under a variety of communication scenarios, from small to large domains, from near to far receivers.

Figure 7(a) shows the decay of maximal coupling strengths (calculated via (10)) for different separation distances d. The source and receiver domains are assumed to be bounded by the sphere-shell geometry with $R_s = R_r = 0.5\lambda$. The filling ratios for both the source and receiver domains are assumed to be at least fifty percent. Figure 7(a) shows all separation distances exhibit sub-exponential decay: the closer the communication domains, the slower their sub-exponential decay. When the receiver is well separated from the source, beyond $d = 10\lambda$, the decay rate does not change. Keeping the two domains separated by $d = 10\lambda$, Fig. 7(b) varies the source domain size R_s from 0.5λ to 20λ and observe more prominent sub-exponential decays for larger domains.

APPENDIX G
POWER-POWER COMMUNICATION MODEL

In Sec. II, we propose two communication models: one rigorous but complex model based on the input-output power relation of antenna systems, and a simpler model based solely on the background Green's function portion of the input-output power relation. We argued above that the latter captures the key physics of the former using (1). In this Appendix, we support this claim with a numerical example: The channel strengths of two concentric metallic shells decay at the same sub-exponential rate for both models. Here we detail our models and calculations.

We first review the complex communication model discussed in Sec. II, which models the full power transmission process from a supplied current $\mathbf{J}_S$ in the source antenna to the induced current $\mathbf{J}_R$ in the receiver antenna. This transmission can be broken down into three steps: 1. the supplied current $\mathbf{J}_S$ induces in the source antenna an induced polarization current $\mathbf{J}'_S = \mathbf{T}'_S\mathbf{J}_S$ through a matrix $\mathbf{T}'_S$, 2. the induced current $\mathbf{J}'_S$ and the supplied current $\mathbf{J}_S$ radiate a field $\mathbf{E} = \mathbf{G}_{RS}(\mathbf{J}'_S + \mathbf{J}_S)$ through the background Green's function $\mathbf{G}_{RS}$, and 3. the field $\mathbf{E}$ induces current $\mathbf{J}_R = \mathbf{T}_R\mathbf{E}$ in the receiver antenna through a matrix $\mathbf{T}_R$. The complete mapping from the supplied current to the induced current in the receiver is $\mathbf{J}_R = \mathbf{T}_R\mathbf{G}_{RS}\mathbf{T}_S\mathbf{J}_S$, where for simplicity we introduce a matrix $\mathbf{T}_S = \mathbf{T}'_S + \mathbf{I}$ that encodes the contribution from both the induced current and the supplied current. The singular value decomposition of the matrix $\mathbf{T}_R\mathbf{G}_{RS}\mathbf{T}_S$ finds a set of orthogonal currents, but with the wrong normalization (not power-normalized) of $|\mathbf{J}_S|^2 = |\mathbf{J}_R|^2 = 1$. Physically the currents should be normalized by the input and output power: $\mathbf{J}_S^\dagger\mathbf{R}_S\mathbf{J}_S = \mathbf{J}_R^\dagger\mathbf{R}_R\mathbf{J}_R = 1$. So the matrix we perform the singular value decomposition should instead be $\mathbf{R}_R^{1/2}\mathbf{T}_R\mathbf{G}_{RS}\mathbf{T}_S\mathbf{R}_S^{-1/2}$. Its singular values define the channel strengths of the power-power communication model.

Given an antenna system, how do we evaluate the matrix $\mathbf{R}_R^{1/2}\mathbf{T}_R\mathbf{G}_{RS}\mathbf{T}_S\mathbf{R}_S^{-1/2}$? The background Green's function matrix $\mathbf{G}_{RS}$ can be easily computed (especially for a vacuum background); the other four matrices, i.e. $\mathbf{R}_R, \mathbf{T}_R, \mathbf{T}_S, \mathbf{R}_S$, need more work. Here, we express them via elementary matrices using the volume equivalence principle [61]. Taking

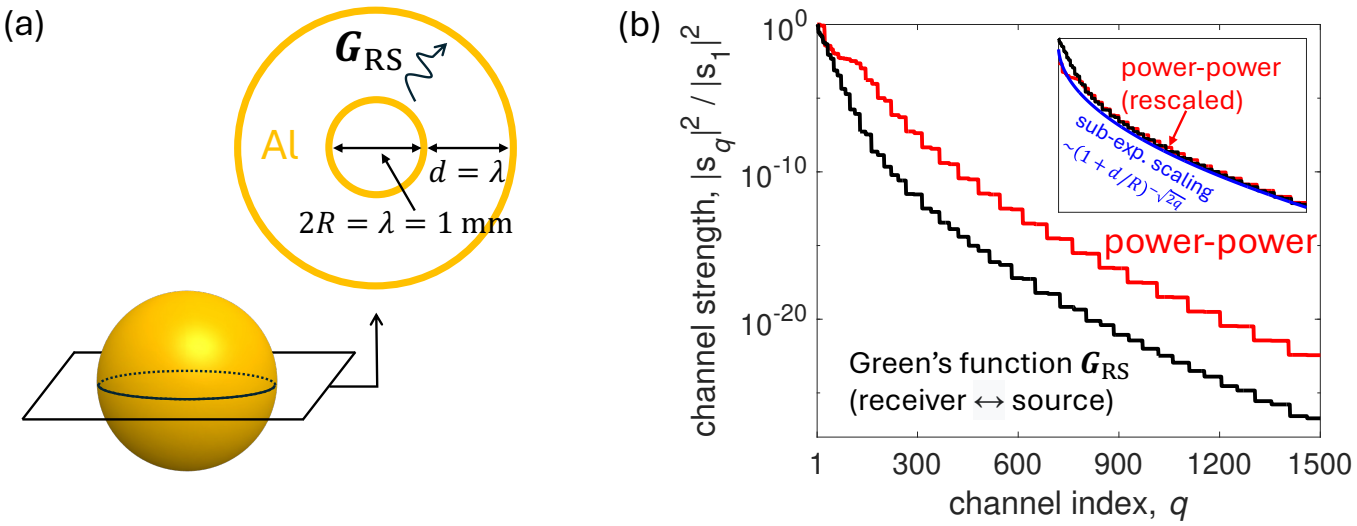

Fig. 8. Power-power communication model. (a) The antenna system is made of two concentric Aluminum shells, separated by distance $d = \lambda = 1$ mm. The inner shell has diameter of $2R = \lambda$. (b) Channel strengths of the power-power communication model and those defined by the Green's function $\mathbf{G}_{SR}$. The two curves have the same sub-exponential scaling, as shown in the inset.

$\mathbf{T}_S$ as an example, the volume equivalent principle states that the field scattered from the source antenna is effectively the radiation of the induced current $\mathbf{J}'_S$ in free space. This radiation plus the incident field has to equal to the total field that induces $\mathbf{J}'_S$ in the source region; this translates to a self-consistent equation:

$$\chi_S \mathbf{G}_{SS}(\mathbf{J}'_S + \mathbf{J}_S) = \mathbf{J}'_S, \tag{42}$$

where $\mathbf{G}_{SS}$ is the background Green's function from the source domain to itself, and χ_S is the susceptibility of the source antenna. This equation implies $\mathbf{T}'_S = (\chi_S^{-1} - \mathbf{G}_{SS})^{-1}\mathbf{G}_{SS}$, and therefore $\mathbf{T}$ is this expression plus an identity. Similarly, the matrix $\mathbf{T}_R$ for the receiver antenna can be written as $\mathbf{T}_R = (\chi_R^{-1} - \mathbf{G}_{RR})^{-1}$, where $\mathbf{G}_{RR}$ is the background Green's function from the receiver domain to itself, and χ_R is the susceptibility of the receiver antenna. (The slight difference between the explicit expressions of $\mathbf{T}_S$ and $\mathbf{T}_R$ is because the former maps from "current" to "current" while the latter maps from "field" to "current".) Just like $\mathbf{G}_{SR}$, the matrices $\mathbf{G}_{SS}$, $\mathbf{G}_{SR}$ and the constants χ_S, χ_R can be easily derived from the antenna material and geometry.

The same elementary matrices also describe the input and output power of the antenna system. The input power equals to the power radiated from the current and the power dissipated inside the material. The former is characterized by the imaginary (anti-Hermitian) part of the Green's function, acting on the total current: $(\mathbf{J}_S + \mathbf{J}'_S)^\dagger \operatorname{Im}\{\mathbf{G}_{SS}\}(\mathbf{J}_S + \mathbf{J}'_S)$; the latter, the imaginary part of the material susceptibility: $(\mathbf{J}_S + \mathbf{J}'_S)^\dagger \operatorname{Im}\{-\chi_R^{-1}\}(\mathbf{J}_S + \mathbf{J}'_S)$. Summing up the two, and converting $\mathbf{J}'_S$ to $\mathbf{J}_S$ using $\mathbf{J}'_S = \mathbf{T}'_S\mathbf{J}_S$, we have $\mathbf{R}_S = \mathbf{T}_S^\dagger \left(\operatorname{Im}\{\mathbf{G}_{SS}\} + \operatorname{Im}\{-\chi_S^{-1}\}\right)\mathbf{T}_S$. Similarly, we write the matrix for the output power as $\mathbf{R}_R = \operatorname{Im}\{-\chi_R^{-1}\}$ which encodes the power dissipated into an external load. (It technically also includes the power dissipated into the receiver material, but that is usually much smaller than the power dissipated into the external load.)

The derived expressions above allow us to evaluate the singular value decomposition of the matrix $\mathbf{R}_R^{1/2}\mathbf{T}_R\mathbf{G}_{RS}\mathbf{T}_S\mathbf{R}_S^{-1/2}$ for most antenna systems. In Fig. 8(a), we consider a system made of two concentric metallic shells. We choose this structure because it captures radiations into all directions, which is expected to be optimal from our model in Fig. 2(a). We choose the radius R of the inner shell to be half a wavelength, and the distance d between shells to be one wavelength (again, similar to Fig. 2(a)). We choose the thickness of both shells to be one tenth of the wavelength. The wavelength λ is 1 mm. The antennas are made of Aluminum. Its susceptibility at this wavelength is $\chi_{\text{Al}} = -8.1 \times 10^4 + i1.9 \times 10^6$ [98]. Consequently, the susceptibility of the receiver antenna is $\chi_S = \chi_{\text{Al}}$. The susceptibility of the receiver antenna, because of the external load, has higher loss. We consider a scenario with a resistive external load that draws $100\times$ as much power as is dissipated in receiver material losses, so that the inverse of the susceptibility (whose imaginary part corresponds to loss) is $\chi_R^{-1} = \operatorname{Re}\{\chi_{\text{Al}}^{-1}\} + i101 \operatorname{Im}\{\chi_{\text{Al}}^{-1}\}$. Lastly, because of the spherical symmetry, we can compute the singular value decomposition more efficiently by decomposing every relevant matrix into vector spherical waves, which are defined in (21-24).

Figure 8(b) compares the singular value of the system's full matrix $\mathbf{R}_R^{1/2}\mathbf{T}_R\mathbf{G}_{RS}\mathbf{T}_S\mathbf{R}_S^{-1/2}$ (red line, labelled power-power) with that of $\mathbf{G}_{RS}$ (black line). The singular values physically represent the channel strengths of the communication channels in both models. Both curves are normalized by the channel strengths of their first channel. The inset re-normalizes the curves to validate their equivalent scalings as a function of channel index. Both the black curve and the re-scaled red curve match the sub-exponential scaling derived in (13). This confirms that our sub-exponential scaling, though derived using a simplified model of the Green's function, applies to realistic considerations of all of the power-transfer

and power-loss pathways in real-material antenna systems..

REFERENCES

[1] David AB Miller. Spatial channels for communicating with waves between volumes. *Optics letters*, 23(21):1645–1647, 1998.

[2] David AB Miller. Communicating with waves between volumes: evaluating orthogonal spatial channels and limits on coupling strengths. *Applied Optics*, 39(11):1681–1699, 2000.

[3] Rafael Piestun and David AB Miller. Electromagnetic degrees of freedom of an optical system. *JOSA A*, 17(5):892–902, 2000.

[4] David AB Miller. Waves, modes, communications, and optics: a tutorial. *Advances in Optics and Photonics*, 11(3):679–825, 2019.

[5] Raffaele Solimene, Claudio Mola, Gianluca Gennarelli, and Francesco Soldovieri. On the singular spectrum of radiation operators in the non-reactive zone: the case of strip sources. *Journal of Optics*, 17(2):025605, 2015.

[6] Giovanni Leone, Maria Antonia Maisto, and Rocco Pierri. Inverse source of circumference geometries: Svd investigation based on fourier analysis. *Progress In Electromagnetics Research M*, 76:217–230, 2018.

[7] Marco Donald Migliore. On the role of the number of degrees of freedom of the field in MIMO channels. *IEEE Transactions on Antennas and Propagation*, 54(2):620–628, 2006.

[8] Giovanni Leone, Fortuna Munno, and Rocco Pierri. Comparison of some geometries in the inverse source problem. In *2019 International Conference on Electromagnetics in Advanced Applications (ICEAA)*, pages 0997–1000. IEEE, 2019.

[9] Giovanni Leone, Fortuna Munno, and Rocco Pierri. Inverse source on conformal conic geometries. *IEEE Transactions on Antennas and Propagation*, 69(3):1596–1609, 2020.

[10] Rocco Pierri and Francesco Soldovieri. On the information content of the radiated fields in the near zone over bounded domains. *Inverse Problems*, 14(2):321, 1998.

[11] Raffaele Solimene and Rocco Pierri. Number of degrees of freedom of the radiated field over multiple bounded domains. *Optics letters*, 32(21):3113–3115, 2007.

[12] Raffaele Solimene, Maria Antonia Maisto, Giuseppe Romeo, and Rocco Pierri. On the singular spectrum of the radiation operator for multiple and extended observation domains. *International Journal of Antennas and Propagation*, 2013, 2013.

[13] Raffaele Solimene, Maria Antonia Maisto, and Rocco Pierri. Role of diversity on the singular values of linear scattering operators: the case of strip objects. *JOSA A*, 30(11):2266–2272, 2013.

[14] Raffaele Solimene, Maria Antonia Maisto, and Rocco Pierri. Inverse source in the presence of a reflecting plane for the strip case. *JOSA A*, 31(12):2814–2820, 2014.

[15] Ada SY Poon, Robert W Brodersen, and David NC Tse. Degrees of freedom in multiple-antenna channels: A signal space approach. *IEEE Transactions on Information Theory*, 51(2):523–536, 2005.

[16] Giovanni Leone, Maria Antonia Maisto, and Rocco Pierri. Application of inverse source reconstruction to conformal antennas synthesis. *IEEE Transactions on Antennas and Propagation*, 66(3):1436–1445, 2018.

[17] Giovanni Leone, Fortuna Munno, and Rocco Pierri. Radiation properties of conformal antennas: The elliptical source. *Electronics*, 8(5):531, 2019.

[18] Radius NS Suryadharma, Martin Fruhnert, Carsten Rockstuhl, and Ivan Fernandez-Corbaton. Singular-value decomposition for electromagnetic-scattering analysis. *Physical Review A*, 95(5):053834, 2017.

[19] Rafael Piestun and C Martijn de Sterke. Fundamental limit for two-dimensional passive devices. *Optics letters*, 34(6):779–781, 2009.

[20] Nicolae Chiurtu and Bixio Rimoldi. Varying the antenna locations to optimize the capacity of multi-antenna gaussian channels. In *2000 IEEE International Conference on Acoustics, Speech, and Signal Processing. Proceedings (Cat. No. 00CH37100)*, volume 5, pages 3121–3123. IEEE, 2000.

[21] Nicolae Chiurtu, Bixio Rimoldi, and Emre Telatar. On the capacity of multi-antenna gaussian channels. In *Proceedings. 2001 IEEE International Symposium on Information Theory (IEEE Cat. No. 01CH37252)*, page 53. IEEE, 2001.

[22] Jon W Wallace and Michael A Jensen. Intrinsic capacity of the MIMO wireless channel. In *Proceedings IEEE 56th Vehicular Technology Conference*, volume 2, pages 701–705. IEEE, 2002.

[23] Michael A Jensen and Jon W Wallace. A review of antennas and propagation for MIMO wireless communications. *IEEE Transactions on antennas and propagation*, 52(11):2810–2824, 2004.

[24] Michael A Jensen and Jon W Wallace. Capacity of the continuous-space electromagnetic channel. *IEEE Transactions on Antennas and Propagation*, 56(2):524–531, 2008.

[25] Mats Gustafsson and Sven Nordebo. On the spectral efficiency of a sphere. *Progress In Electromagnetics Research*, 67:275–296, 2007.

[26] Andrés Alayon Alayon Glazunov, Mats Gustafsson, and Andreas F Molisch. On the physical limitations of the interaction of a spherical aperture and a random field. *IEEE transactions on antennas and propagation*, 59(1):119–128, 2010.

[27] David Slepian and Henry O Pollak. Prolate spheroidal wave functions, fourier analysis and uncertainty—i. *Bell System Technical Journal*, 40(1):43–63, 1961.

[28] G Do Boyd and Jo Po Gordon. Confocal multimode resonator for millimeter through optical wavelength masers. *Bell System Technical Journal*, 40(2):489–508, 1961.

[29] B Roy Frieden. Viii evaluation, design and extrapolation methods for optical signals, based on use of the prolate functions. In *Progress in optics*, volume 9, pages 311–407. Elsevier, 1971.

[30] M Bertero and ER Pike. Resolution in diffraction-limited imaging, a singular value analysis. *Optica Acta: International Journal of Optics*, 29(6):727–746, 1982.

[31] Arthur G Fox and Tingye Li. Resonant modes in a maser interferometer. *Bell System Technical Journal*, 40(2):453–488, 1961.

[32] David AB Miller. Fundamental limit for optical components. *JOSA B*, 24(10):A1–A18, 2007.

[33] David AB Miller. Fundamental limit to linear one-dimensional slow light structures. *Physical review letters*, 99(20):203903, 2007.

[34] David AB Miller, Linxiao Zhu, and Shanhui Fan. Universal modal radiation laws for all thermal emitters. *Proceedings of the National Academy of Sciences*, 114(17):4336–4341, 2017.

[35] Emre Telatar. Capacity of multi-antenna gaussian channels. *European transactions on telecommunications*, 10(6):585–595, 1999.

[36] Andrea Goldsmith, Syed Ali Jafar, Nihar Jindal, and Sriram Vishwanath. Capacity limits of MIMO channels. *IEEE Journal on selected areas in Communications*, 21(5):684–702, 2003.

[37] David Tse and Pramod Viswanath. *Fundamentals of wireless communication*. Cambridge university press, 2005.

[38] Ivo M Vellekoop and AP Mosk. Focusing coherent light through opaque strongly scattering media. *Optics letters*, 32(16):2309–2311, 2007.

[39] Per Martinsson, Ping Ma, Anna Burvall, and Ari T Friberg. Communication modes in scalar diffraction. *Optik*, 119(3):103–111, 2008.

[40] Sébastien M Popoff, Geoffroy Lerosey, Rémi Carminati, Mathias Fink, Albert Claude Boccara, and Sylvain Gigan. Measuring the transmission matrix in optics: an approach to the study and control of light propagation in disordered media. *Physical review letters*, 104(10):100601, 2010.

[41] David AB Miller. Establishing optimal wave communication channels automatically. *Journal of Lightwave Technology*, 31(24):3987–3994, 2013.

[42] David AB Miller. Self-configuring universal linear optical component. *Photonics Research*, 1(1):1–15, 2013.

[43] Guifang Li, Neng Bai, Ningbo Zhao, and Cen Xia. Space-division multiplexing: the next frontier in optical communication. *Advances in Optics and Photonics*, 6(4):413–487, 2014.

[44] Ningbo Zhao, Xiaoying Li, Guifang Li, and Joseph M Kahn. Capacity limits of spatially multiplexed free-space communication. *Nature photonics*, 9(12):822–826, 2015.

[45] David AB Miller. Better choices than optical angular momentum multiplexing for communications. *Proceedings of the National Academy of Sciences*, 114(46):E9755–E9756, 2017.

[46] Andrea Annoni, Emanuele Guglielmi, Marco Carminati, Giorgio Ferrari, Marco Sampietro, David AB Miller, Andrea Melloni, and Francesco Morichetti. Unscrambling light—automatically undoing strong mixing between modes. *Light: Science & Applications*, 6(12):e17110–e17110, 2017.

[47] Hasan Yılmaz, Chia Wei Hsu, Alexey Yamilov, and Hui Cao. Transverse localization of transmission eigenchannels. *Nature Photonics*, 13(5):352–358, 2019.

[48] Claude Elwood Shannon. A mathematical theory of communication. *The Bell system technical journal*, 27(3):379–423, 1948.

[49] David Slepian. On bandwidth. *Proceedings of the IEEE*, 64(3):292–300, 1976.

[50] Joseph W Goodman. *Introduction to Fourier optics*. Roberts and Company publishers, 2005.

[51] Denis Gabor. Iv light and information. In *Progress in optics*, volume 1, pages 109–153. Elsevier, 1961.

[52] G Toraldo di Francia. Resolving power and information. *Journal of the Optical Society of America*, 45(7):497–501, 1955.

[53] O. Bucci and G. Franceschetti. On the spatial bandwidth of scattered fields. *IEEE Transactions on Antennas and Propagation*, 35(12):1445–1455, 1987.

[54] Ovidio M Bucci and Giorgio Franceschetti. On the degrees of freedom of scattered fields. *IEEE transactions on Antennas and Propagation*, 37(7):918–926, 1989.

[55] Leif Hanlen and Minyue Fu. Wireless communication systems with-spatial diversity: A volumetric model. *IEEE Transactions on Wireless Communications*, 5(1):133–142, 2006.

[56] Myungjun Lee, Mark A Neifeld, and Amit Ashok. Capacity of electromagnetic communication modes in a noise-limited optical system. *Applied Optics*, 55(6):1333–1342, 2016.

[57] Casimir Ehrenborg and Mats Gustafsson. Fundamental bounds on MIMO antennas. *IEEE Antennas and Wireless Propagation Letters*, 17(1):21–24, 2017.

[58] Casimir Ehrenborg and Mats Gustafsson. Physical bounds and radiation modes for MIMO antennas. *IEEE Transactions on Antennas and Propagation*, 68(6):4302–4311, 2020.

[59] Casimir Ehrenborg, Mats Gustafsson, and Miloslav Capek. Capacity bounds and degrees of freedom for MIMO antennas constrained by q-factor. *IEEE Transactions on Antennas and Propagation*, 2021.

[60] Zeyu Kuang. *Fundamental Limits of Nanophotonic Design*. Yale University, 2023.

[61] Jian-Ming Jin. *Theory and computation of electromagnetic fields*. John Wiley & Sons, 2011.

[62] George W Hanson and Alexander B Yakovlev. *Operator theory for electromagnetics: an introduction*, chapter 4.2.1, page 232. Springer Science & Business Media, 1 edition, 2002.

[63] Sean Molesky, Prashanth S Venkataram, Weiliang Jin, and Alejandro W Rodriguez. Fundamental limits to radiative heat transfer: Theory. *Physical Review B*, 101(3):035408, 2020.

[64] Milton Abramowitz and Irene A Stegun. *Handbook of mathematical functions with formulas, graphs, and mathematical tables*, volume 55, chapter 9, page 363. US Government printing office, 1964.

[65] John David Jackson. Classical electrodynamics, 1999.

[66] Leung Tsang, Jin Au Kong, and Kung-Hau Ding. *Scattering of electromagnetic waves: theories and applications*. John Wiley & Sons, 2004.

[67] Owen D Miller, Steven G Johnson, and Alejandro W Rodriguez. Shape-independent limits to near-field radiative heat transfer. *Physical review letters*, 115(20):204302, 2015.

[68] Prashanth S Venkataram, Sean Molesky, Weiliang Jin, and Alejandro W Rodriguez. Fundamental limits to radiative heat transfer: The limited role of nanostructuring in the near-field. *Physical review letters*, 124(1):013904, 2020.

[69] Per-Simon Kildal, Enrica Martini, and Stefano Maci. Degrees of freedom and maximum directivity of antennas: A bound on maximum directivity of nonsuperreactive antennas. *IEEE Antennas and Propagation Magazine*, 59(4):16–25, 2017.

[70] Andreas F Molisch and Moe Z Win. MIMO systems with antenna selection. *IEEE microwave magazine*, 5(1):46–56, 2004.

[71] Andreas F Molisch, Moe Z Win, Yang-Seok Choi, and Jack H Winters. Capacity of MIMO systems with antenna selection. *IEEE Transactions on Wireless Communications*, 4(4):1759–1772, 2005.

[72] Yuan Gao, Han Vinck, and Thomas Kaiser. Massive MIMO antenna selection: Switching architectures, capacity bounds, and optimal antenna selection algorithms. *IEEE Transactions on Signal Processing*, 66(5):1346–1360, 2017.

[73] Saba Asaad, Amir Masoud Rabiei, and Ralf R Müller. Massive MIMO with antenna selection: Fundamental limits and applications. *IEEE Transactions on Wireless Communications*, 17(12):8502–8516, 2018.

[74] Andreas F Molisch, Alexander Kuchar, Juha Laurila, Klaus Hugl, and Ralph Schmalenberger. Geometry-based directional model for mobile radio channels—principles and implementation. *European Transactions on Telecommunications*, 14(4):351–359, 2003.

[75] Peter Almers, Ernst Bonek, Alister Burr, Nicolai Czink, Mérouane Debbah, Vittorio Degli-Esposti, Helmut Hofstetter, Pekka Kyösti, David Laurenson, Gerald Matz, et al. Survey of channel and radio propagation models for wireless MIMO systems. *EURASIP Journal on Wireless Communications and Networking*, 2007:1–19, 2007.

[76] Viktar S Asadchy, Mohammad Sajjad Mirmoosa, Ana Diaz-Rubio, Shanhui Fan, and Sergei A Tretyakov. Tutorial on electromagnetic nonreciprocity and its origins. *Proceedings of the IEEE*, 108(10):1684–1727, 2020.

[77] Emanuele Galiffi, Romain Tirole, Shixiong Yin, Huanan Li, Stefano Vezzoli, Paloma A Huidobro, Mário G Silveirinha, Riccardo Sapienza, Andrea Alù, and JB Pendry. Photonics of time-varying media. *Advanced Photonics*, 4(1):014002–014002, 2022.

[78] Shixiong Yin, Emanuele Galiffi, Gengyu Xu, and Andrea Alù. Scattering at temporal interfaces: An overview from an antennas and propagation engineering perspective. *IEEE Antennas and Propagation Magazine*, 2023.

[79] Christian Sohl, Mats Gustafsson, and Gerhard Kristensson. Physical limitations on broadband scattering by heterogeneous obstacles. *Journal of Physics A: Mathematical and Theoretical*, 40(36):11165, 2007.

[80] Zongfu Yu, Aaswath Raman, and Shanhui Fan. Fundamental limit of nanophotonic light trapping in solar cells. *Proceedings of the National Academy of Sciences*, 107(41):17491–17496, 2010.

[81] Hanwen Zhang, Chia Wei Hsu, and Owen D Miller. Scattering concentration bounds: brightness theorems for waves. *Optica*, 6(10):1321–1327, 2019.

[82] Federico Presutti and Francesco Monticone. Focusing on bandwidth: achromatic metalens limits. *Optica*, 7(6):624–631, 2020.

[83] Hyungki Shim, Haejun Chung, and Owen D Miller. Maximal free-space concentration of electromagnetic waves. *Physical Review Applied*, 14(1):014007, 2020.

[84] Yi Yang, Aviram Massuda, Charles Roques-Carmes, Steven E Kooi, Thomas Christensen, Steven G Johnson, John D Joannopoulos, Owen D Miller, Ido Kaminer, and Marin Soljačić. Maximal spontaneous photon emission and energy loss from free electrons. *Nature Physics*, 14(9):894–899, 2018.

[85] Owen D Miller, Athanasios G Polimeridis, MT Homer Reid, Chia Wei Hsu, Brendan G DeLacy, John D Joannopoulos, Marin Soljačić, and Steven G Johnson. Fundamental limits to optical response in absorptive systems. *Optics express*, 24(4):3329–3364, 2016.

[86] Owen D Miller, Ognjen Ilic, Thomas Christensen, MT Homer Reid, Harry A Atwater, John D Joannopoulos, Marin Soljačić, and Steven G Johnson. Limits to the optical response of graphene and two-dimensional materials. *Nano letters*, 17(9):5408–5415, 2017.

[87] Sean Molesky, Pengning Chao, Weiliang Jin, and Alejandro W Rodriguez. Global T operator bounds on electromagnetic scattering: Upper bounds on far-field cross sections. *Physical Review Research*, 2(3):033172, 2020.

[88] Mats Gustafsson, Kurt Schab, Lukas Jelinek, and Miloslav Capek. Upper bounds on absorption and scattering. *New Journal of Physics*, 22(7):073013, 2020.

[89] Zeyu Kuang, Lang Zhang, and Owen D Miller. Maximal single-frequency electromagnetic response. *Optica*, 7(12):1746–1757, 2020.

[90] Sean Molesky, Pengning Chao, and Alejandro W Rodriguez. Hierarchical mean-field T operator bounds on electromagnetic scattering: Upper bounds on near-field radiative purcell enhancement. *Physical Review Research*, 2(4):043398, 2020.

[91] Zeyu Kuang and Owen D Miller. Computational bounds to light–matter interactions via local conservation laws. *Physical Review Letters*, 125(26):263607, 2020.

[92] Hyungki Shim, Lingling Fan, Steven G Johnson, and Owen D Miller. Fundamental limits to near-field optical response over any bandwidth. *Physical Review X*, 9(1):011043, 2019.

[93] Sean Molesky, Weiliang Jin, Prashanth S Venkataram, and Alejandro W Rodriguez. T operator bounds on angle-integrated absorption and thermal radiation for arbitrary objects. *Physical review letters*, 123(25):257401, 2019.

[94] Sean Molesky, Pengning Chao, Jewel Mohajan, Wesley Reinhart, Heng Chi, and Alejandro W Rodriguez. T-operator limits on optical communication: Metaoptics, computation, and input-output transformations. *Physical Review Research*, 4(1):013020, 2022.

[95] Hyungki Shim, Zeyu Kuang, Zin Lin, and Owen D Miller. Fundamental limits to multi-functional and tunable nanophotonic response. *Nanophotonics*, 13(12):2107–2116, 2024.

[96] Mats Gustafsson. Degrees of freedom for radiating systems. *arXiv preprint arXiv:2404.08976*, 2024.

[97] Mats Gustafsson. Shadow area and degrees-of-freedom for free-space communication. *arXiv preprint arXiv:2407.21122*, 2024.

[98] H-J Hagemann, W Gudat, and C Kunz. Optical constants from the far infrared to the x-ray region: Mg, al, cu, ag, au, bi, c, and al 2 o 3. *JOSA*, 65(6):742–744, 1975.